

was made by Crittenden *et al.*⁷ using known resonances in the πp system and their Regge recurrences up to 1860 MeV. The curve in Fig. 3 is the result of calculation at 2.28 GeV/c using the model of Ref. 6. The curve is not normalized to our data and the agreement is excellent.

ACKNOWLEDGMENTS

We wish to thank Dr. Y. L. Pan for his valuable

assistance throughout the experiment. We would especially like to thank Professor J. D. Kimel for his help in the calculations. We would like to acknowledge helpful discussions with Professor P. K. Williams and J. Lannutti. We are grateful for the support of the staff of the Princeton-Pennsylvania Accelerator and Bubble Chamber. Also our thanks to the staffs of the University of Pennsylvania Hough-Powell Device and the high-energy computing center.

*Work supported in part by the U. S. Atomic Energy Commission.

†Before 1970 at University of Pennsylvania, Philadelphia, Pennsylvania.

‡Present address: Department of Radiology, University of Pennsylvania, Philadelphia, Pennsylvania.

§Present address: Mitre Corporation, Bedford, Massachusetts.

¹S. Hagopian *et al.*, Phys. Rev. Letters **24**, 1445 (1970); **25**, 1050 (1970).

²B. G. Reynolds *et al.*, Phys. Rev. **173**, 1403 (1968).

³R. E. Hill *et al.*, Phys. Rev. D **1**, 729 (1970). Other

relevant references are found in this paper.

⁴More information on this experiment can be obtained from theses of S. Hagopian and R. O'Donnell, University of Pennsylvania, 1970 (unpublished).

⁵A. Diddens *et al.*, Phys. Rev. Letters **10**, 262 (1963).

⁶G. Höhler, G. Ebel, and J. Giesecke, Z. Physik **180**, 430 (1964).

⁷R. R. Crittenden *et al.*, Phys. Rev. D **1**, 3050 (1970), based on a model by R. R. Crittenden *et al.*, *ibid.* **1**, 169 (1970). For other backward scattering data see also A. S. Carroll *et al.*, Phys. Rev. Letters **20**, 607 (1968); S. W. Kormanyos *et al.*, *ibid.* **16**, 709 (1966).

Investigation of Low-Mass $K\pi\pi$ Systems in 12-GeV/c K^+p Interactions*

Philip J. Davis, Margaret Alston-Garnjost, Angela Barbaro-Galtieri,
Stanley M. Flatté, Jerome H. Friedman, Gerald R. Lynch,
Monroe S. Rabin, and Frank T. Solmitz

Lawrence Berkeley Laboratory, University of California, Berkeley, California 94720

(Received 10 December 1971)

We have studied the broad $K\pi\pi$ mass enhancements at 1300 MeV in the reactions $K^+p \rightarrow pK^+\pi^-\pi^+$ and $pK^0\pi^0\pi^+$ at 12 GeV/c. Our data were obtained from a 600 000-picture exposure of the SLAC 82-in. hydrogen bubble chamber (which corresponds to a path length of 35 events/ μb). We observe a two-peak substructure in the $K^0\pi^0\pi^+$ mass spectrum at 1260 and 1420 MeV. Our estimated contribution of the $K_N(1420)$ accounts for only about half of the 1420-MeV peak (a discrepancy of about 2.4 standard deviations). The $K^+\pi^-\pi^+$ mass spectrum has a different shape. Further, assuming the $K\pi\pi$ system to be S wave $1^+K_Y(890)\pi$ and $\rho(765)K$, we have fitted separately the $K^+\pi^-\pi^+$ and the $K^0\pi^0\pi^+$ Dalitz plots. We obtain inconsistent fits. This inconsistency and the differences in the $K\pi\pi$ mass spectra could be explained by an additional contribution of an $I=0$ S-wave $\pi\pi$ state in $K^+\pi^-\pi^+$. The $K\pi\pi$ angular decay distributions imply the dominance of the spin-parity state 1^+ with $M_x=0$ along the incident beam direction. However, there are other J^P states and states with $M_x \neq 0$. The 1260-MeV $K\pi\pi$ mass region is produced more peripherally than the 1420-MeV region.

I. INTRODUCTION

A. Purpose and Scope

The $K\pi\pi$ 1.3-GeV mass region, the Q , has been extensively studied.¹⁻²⁹ (See Ref. 1 for a compilation.) Despite this effort, questions of the exis-

tence and/or nature of Q substructure remain unsettled. Interest in Q substructure is due in part to the possible assignments of two resonances to SU(3) nonets with $J^{PC} = 1^{++}$. In the hope of obtaining additional results regarding Q substructure, we analyze the 12-GeV/c K^+p reactions:

- | | |
|--|----------------|
| (1) $K^+p \rightarrow pK^+\pi^-\pi^+$, | 30 163 events, |
| (2) $K^+p \rightarrow pK^0\pi^0\pi^+$, $K^0 \rightarrow \pi^-\pi^+$, | 6431 events, |
| (3) $K^+p \rightarrow nK^0\pi^+\pi^+$, $K^0 \rightarrow \pi^-\pi^+$, | 1279 events, |
| (4) $K^+p \rightarrow pK^0\pi^+$, $K^0 \rightarrow \pi^-\pi^+$, | 1900 events. |

The data are from 600 000 pictures of the SLAC 82-in. hydrogen bubble chamber exposed to an rf-separated 12-GeV/c K^+ beam.³⁰ For reactions (1) and (2) we select events with $M(K\pi\pi) < 1.5$ GeV. Reaction (3) is analyzed to corroborate the Q isospin assignment of $\frac{1}{2}$. Reaction (4) is used to determine the $K_N(1420)$ contributions to reactions (1) and (2).

We conclude our introduction with a brief synopsis of the existing Q data and a summary of our results. In Sec. II we discuss the data reduction and emphasize the problem of $K^+\pi^+$ ambiguity in reaction (1). Section III deals first with the $K\pi\pi$ mass spectra, secondly with the failure of the $K_N(1420)$ to account fully for our observed $K^0\pi^0\pi^+$ mass structure, and thirdly with detailed studies, including Dalitz-plot fits. In Sec. IV we summarize our results and compare them with three similar experiments.

B. Brief Synopsis of Existing Q Data

The existing Q data are derived from two basic sets of experiments: first, those which observe a diffractive $K\pi\pi$ enhancement in a reaction of the kind $KT \rightarrow K\pi\pi T$, where T is some target; and secondly, those which observe a $K\pi\pi$ enhancement in nondiffractive reactions. The first experiments agree generally that (1) the Q is a broad $K\pi\pi$ enhancement peripherally produced, (2) the Q decays predominately into $K_V(890)\pi$ but also into $\rho(765)K$, (3) the Q has isospin $\frac{1}{2}$, and (4) the Q has spin-parity 1^+ favored, but with 2^- still possible. These same experiments differ in their conclusions regarding Q structure. Several report two or more resonances in the Q region.^{7, 8, 29} Some report structure with a 1420-MeV peak accounted for by the $K_N(1420)$.^{17, 27} In contrast, other experiments report that the $K_N(1420)$ fails to account fully for their observed 1420-MeV peak.^{14, 25} In contrast to a resonant interpretation, several experiments obtain reasonable fits to their data by Deck or double-Regge-pole models, e.g., diffractive dissociation of the beam into $K_V(890)\pi$ with the π then elastically scattering off the target.^{12, 15, 20, 22} [Usually the $K_V(890)\pi$ mass spectrum is the least well fitted kinematic variable.] Because of duality, the resonant and Deck descriptions may be theoretically compatible.³¹ At the 1970 Philadelphia Conference, Firestone reviewed the K^+p experiments from 2.15 to 13 GeV/c.²⁸ By fitting the $K\pi\pi$ mass distributions, he concluded that a simple Breit-Wigner shape does not fit the

Q peak, but that two Breit-Wigner shapes do give reasonable fits at all energies.

Besides the above diffractive experiments, there are some nondiffractive experiments with either a \bar{p} or π^- beam.²⁻⁵ Most significant among these is that of Astier *et al.*⁴ who find evidence in $\bar{p}p \rightarrow \bar{K}K\pi\pi$ for a $K\pi\pi$ resonance, the C meson, with a mass and width of 1242^{+9}_{-10} MeV and 127^{+7}_{-25} MeV. The C -meson branching ratios into $K_V(890)\pi$ and $\rho(765)K$ are (0.25 ± 0.1) and (0.75 ± 0.1) . They assign to the C meson the quantum numbers $J^{PC} = 1^{++}$. Crennell *et al.*³ find evidence for production of two $K\pi\pi$ enhancements in $\pi^-p \rightarrow \Lambda K\pi\pi$ at 6 GeV/c: one at about 1440 MeV, which they associate with the $K_N(1420)$; and the other at about 1300 MeV. They favor a resonant interpretation for the 1300-MeV enhancement and assign it a narrow width of about 60 MeV, an isospin of $\frac{1}{2}$, and decay modes into both $K_V(890)$ and $\rho(765)K$.

In summary, the diffractive experiments have generally broad $K\pi\pi$ enhancements, either with or without substructure. The relatively narrow enhancements seen by Astier *et al.* and Crennell *et al.* complicate the interpretation of the diffractive Q data.

C. Results

We find evidence for a two-peak $K^0\pi^0\pi^+$ mass spectrum (see Fig. 1). The low- Q peak, which

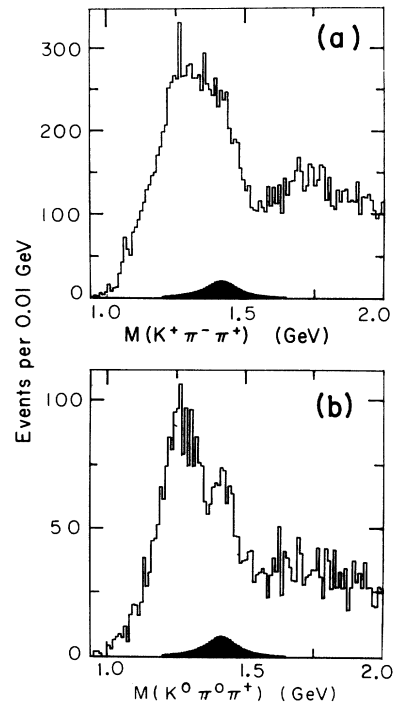


FIG. 1. The $K\pi\pi$ mass spectra with no cuts for $K^+p \rightarrow pK^+\pi^-\pi^+$ and $pK^0\pi^0\pi^+$. The shaded areas are the estimated $K_N(1420)$ contributions of 360 and 140 events in $K^+\pi^-\pi^+$ and $K^0\pi^0\pi^+$.

we shall label Q_L , is centered at about 1260 MeV with a full-width of about 120 MeV, and the high- Q peak, which we shall label Q_H , is centered at about 1420 MeV with a full-width of about 80 MeV. These values are quite dependent upon the assumed background. Using the known $K_N(1420)$ branching ratios and the amount of $K_N(1420) \rightarrow K^0\pi^+$ determined for reaction (4), we calculate the $K_N(1420)$ contributions to the $K\pi\pi$ mass spectra (see the shaded areas of Fig. 1). The $K_N(1420)$ accounts only for about half of the observed $K^0\pi^0\pi^+$ peak at 1420 MeV. The $K^+\pi^-\pi^+$ spectrum has a shape different from that of $K^0\pi^0\pi^+$. The differences in the $K\pi\pi$ mass spectra may be explained by a contribution to the Q of $\epsilon(700)K$, $\epsilon(700) \rightarrow \pi^-\pi^+$, where by $\epsilon(700)$ we mean only an isospin-0 S -wave $\pi\pi$ state and not necessarily a resonance. The $\epsilon(700)K$ can contribute to $K^+\pi^-\pi^+$, but not to $K^0\pi^0\pi^+$. The ratio of the number of $K^0\pi^0\pi^+$ to $K^+\pi^-\pi^+$ events gives added support for an $\epsilon(700)K$ mode. For pure $\epsilon(700)K$, $\rho(765)K$, and $K_V(890)\pi$, this ratio would be 0, 2, and 1, respectively. Despite the presence of significant $\rho(765)K$ in our data, the ratio is unity within errors (6%) for four Q mass subdivisions. This result is similar to that obtained by Alexander *et al.*¹⁴ who originally suggested the possible contribution of the $\epsilon(700)K$.

Our Q decay-plane-normal distributions and the $Q \rightarrow K(890)\pi$, $K_V(890) \rightarrow K^+\pi^-$ two-body angular decay distributions imply that $J^P = 1^+$ is favored. However, we can exclude neither $J^P = 0^-$ nor 2^- . With the assumption that the Q is in a $J^P = 1^+$ state, an analysis of the $Q \rightarrow K_V(890)\pi$, $K_V(890) \rightarrow K^+\pi^-$ two-body angular decay distributions indicates that the $Q \rightarrow K_V(890)\pi$ decay is predominantly S wave with zero spin projection along the beam, $M_z = 0$. However, the Q has significant non- S -wave 1^+ components and significant components with $M_z \neq 0$.

We determine the Q decay modes by fitting separately the $K^+\pi^-\pi^+$ and $K^0\pi^0\pi^+$ Dalitz plots to S wave 1^+ $K_V(890)\pi$ and $\rho(765)K$ for four $K\pi\pi$ mass subdivisions. We perform both incoherent and partially coherent fits. Interference effects are

important. The fraction of $\rho(765)K$ in $K^0\pi^0\pi^+$ ranges between 0.24 ± 0.06 and 0.37 ± 0.05 for different $K\pi\pi$ mass regions. Using the $K^0\pi^0\pi^+$ fitted results and assuming pure S wave 1^+ , we estimate that the $\epsilon(700)K$ contribution in $K^+\pi^-\pi^+$ consists of a fraction ranging from 0.03 ± 0.08 to 0.22 ± 0.06 , the lower values applying to low $K\pi\pi$ masses and the higher to the 1420-MeV region.

II. DATA REDUCTION

A. Scanning and Measuring

All pictures were at least twice-scanned and 10% of the film was thrice-scanned.³² Reaction (1) corresponds to a four-prong topology. Reactions (2) through (4) correspond to a vee-two-prong topology. We use the Derenzo-Hildebrand method to calculate scan efficiencies.³³ (For our experiment this method yields slightly smaller values than the traditional Geiger-Werner method.) The first-scan four-prong and vee-two-prong efficiencies are 0.97 and 0.90.³⁴ With exclusion of nonbeam events and measurer rejects of invalid events, a total of about 189 000 four prongs and 38 000 vee-two prongs were measured with the Spiral Reader. The LBL Group A programs – POOH, TVGP, and SQUAW – were used in the data reduction. Failing events were measured a second time, and of the twice-failing events, half were measured a third time.³⁵ The measuring and scanning results are summarized in Table I.

B. Path Length

Three methods are used in calculating the path length.³⁴ They use, respectively: (1) the number of τ decays, (2) the number and length of beam tracks, and (3) the total number of events normalized to the known total cross section. These three methods give for the path length, respectively, 34.7 ± 0.9 , 35.2 ± 0.6 , and 34.0 ± 1.2 events/ μb . The weighted average is 34.9 ± 0.5 events/ μb . (Small correlations are neglected.) The weighted average has a χ^2 of 0.8 for 2 degrees of freedom. Despite this good agreement we use as our final

TABLE I. Summary of data reduction.

	Four-prongs	Vee two-prongs
No. of events	189 000	38 000
First-scan efficiency	0.97	0.91
Double-scan efficiency	1.00	0.99
First-measurement efficiency	0.738 ± 0.008	0.67 ± 0.02
Net measurement efficiency ^a	0.897 ± 0.013	0.846 ± 0.026

^a The fraction of events passing, after at least two measurements of all failing events and three measurements for half of the twice-failing events.

answer 34.9 ± 1.0 events/ μb , because of possible systematic errors in our results. Table II is a summary of the cross sections for reactions (1) through (4) calculated using the efficiencies and path length in Table I.

C. Fit Ambiguities

1. Final State $pK^+\pi^-\pi^+$

All successfully measured four-prong events are fitted to the final-state hypotheses: (a) $pK^+\pi^-\pi^+$, (b) $pK^+K^-K^+$, and (c) $pK^+\bar{p}p$. The best fit is defined as the fit with the minimum sum of kinematic χ_K^2 and bubble-density χ_{BD}^2 . χ_{BD}^2 is calculated using the pulse-height information of Spiral Reader measurements.³⁶ In addition, a fit is required to have a χ_K^2 corresponding to a confidence level greater than 10^{-5} .

Best fits to $pK^+\pi^-\pi^+$ have a 26% ambiguity including permutations of the track identities. For our study of the Q region we selected events with $M(K\pi\pi) < 1.5$ GeV and $M(p\pi^+) > 1.5$ GeV. The $p\pi^+$ mass cut removes events with a $\Delta^{++}(1236)$ present. With these selections, best fits to $pK^+\pi^-\pi^+$ have a 40% permutation ambiguity, a 3% ambiguity with $pK^+K^-K^+$, and a 4% ambiguity with $pK^+\bar{p}p$ (see Table III). We proceed to discuss each of these ambiguities in detail. Since the Q is produced peripherally, the outgoing proton is easily identified; but interchanging the K^+ and π^+ identifications results only in a slight change of the energy balance when the K^+ and π^+ have nearly the same lab momentum. Likewise, since the K^+ and π^+ are usually both minimum ionizing, there is little difference in the χ_{BD}^2 for permutation ambiguities.

To estimate the fraction and effects of having the wrong permutation fit best, we generate two Monte Carlo samples of track measurements and then process them as actual measurements.³⁷ The first Monte Carlo sample corresponds to a

TABLE II. Cross sections for 12-GeV/c K^+p .

Reaction	No. of events	Cross section (μb)
(1) $K^+p \rightarrow pK^+\pi^-\pi^+$		
No cuts	30 163	935 ± 30
$M(K\pi\pi) < 1.5$ GeV	8961	278 ± 9
$M(K\pi\pi) < 1.5$ GeV $M(p\pi^+) > 1.5$ GeV $-t_{pp} < 1$ GeV ²	7687	238 ± 8
(2) $K^+p \rightarrow pK^0\pi^0\pi^+$		
No cuts	6431	650 ± 28
$M(K\pi\pi) < 1.5$ GeV	2283	231 ± 11
$M(K\pi\pi) < 1.5$ GeV $M(p\pi^+) > 1.5$ GeV $-t_{pp} < 1$ GeV ²	1919	194 ± 9
(3) $K^+p \rightarrow nK^0\pi^+\pi^+$		
No cuts	1279	129 ± 6
$M(K\pi\pi) < 1.5$ GeV $-t_{pn} < 1$ GeV ²	126	13 ± 1
(4) $K^+p \rightarrow pK^0\pi^+$		
No cuts	1900	246 ± 11

$K^+\pi^-\pi^+$ resonance peripherally produced (e^3p_p), and with a mass of 1300 MeV, a width of 300 MeV, and an S-wave decay into $K_V(890)\pi$. The $K_V(890)$ decay into $K^+\pi^-$ is given a $\cos^2\theta$ distribution with respect to the beam. As with the data, we require a $M(K\pi\pi) < 1.5$ GeV and a $M(p\pi^+) > 1.5$ GeV. Of 439 generated events, 42% have a permutation ambiguity. Of these ambiguities, (19 \pm 3)% have the wrong permutation fitting best. The second Monte Carlo sample corresponds to an analogous $\rho(765)K$ decay of the Q . Of 438 generated events, 47% have a permutation ambiguity of which (15 \pm 3)% have the wrong permutation fitting best. Therefore we estimate that 8% of all $K^+\pi^-\pi^+$ events in the Q region are ambiguous with the wrong permutation

TABLE III. Fit-ambiguity results for Q events.^a

A. Best fit to $pK^+\pi^-\pi^+$	Percent with second best fit to:			Total
	$pK^+\pi^-\pi^+$ ^b	$pK^+K^-K^+$	$pK^+\bar{p}p$	
Without χ_{BD}^2 selection	40%	3%	4%	47%
With χ_{BD}^2 selection ^c	40	1	2	43
B. Best fit to $pK^0\pi^0\pi^+$	Percent with second best fit to:			Total
	$pK^0K^0K^+$	$nK^0K^+K^+$		
With χ_{BD}^2 selection ^c	3%	5%		9%

^a The Q selection is $M(K\pi\pi) < 1.5$ GeV and $M(p\pi^+) > 1.5$ GeV.

^b For $pK^+\pi^-\pi^+$ vs $pK^+K^-K^+$, the 40% corresponds to track permutation ambiguities.

^c The bubble-density χ^2 selection is that the χ_{BD}^2 be less than five plus the minimum χ_{BD}^2 of all fits.

fitting best. In addition, we find for the two Monte Carlo samples, respectively, that $(1.6 \pm 0.6)\%$ and $(0.7 \pm 0.4)\%$ of generated Q events have a wrong permutation fit passing and the correct permutation fit failing. Thus, we estimate that about 10% of all real $K^+\pi^-\pi^+$ events in the Q region correspond to the wrong $K^+\pi^+$ permutation.

The $K^+\pi^+$ misidentification produces a serious bias in our $K^+\pi^-\pi^+$ data for the Q . The above Monte Carlo samples indicate that actual $K_V(890)\pi$ events with $K^+\pi^+$ misidentification result in a $\pi^-\pi^+$ mass peaking at about 720 MeV, and in a fairly uniform $K^+\pi^-$ mass spectrum. Wrongly identified $\rho(765)K$ events result in a $K^+\pi^-$ mass spectrum spread out between 780 and 1000 MeV, and in a $\pi^-\pi^+$ mass spectrum spread out between 440 and 810 MeV. For the $K_V(890)\pi$ misidentification, the $K\pi\pi$ mass has an average shift of +10 MeV with a spread of ± 20 MeV.

Best fits to $pK^+\pi^-\pi^+$ ambiguous with $pK^+K^-K^+$ or $pK^+\bar{p}p$ comprise 7% of all $K^+\pi^-\pi^+$ events in the Q region. After examining a sample of these ambiguities on the scan table, we decided that by a selection upon χ_{BD}^2 , we could reduce the contamination of $pK^+K^-K^+$ and $pK^+\bar{p}p$ to 1% and 2%, respectively (see Table III).

2. Final States $pK^0\pi^0\pi^+$ and $nK^0\pi^+\pi^+$

Both final states $pK^0\pi^0\pi^+$ and $nK^0\pi^+\pi^+$ correspond to a vee-two-prong topology with a one-constraint (1C) fit at the production vertex and a 3C fit at the vee vertex for the K^0 decay into $\pi^-\pi^+$. A special study of ambiguities led to the following selection criteria for production 1C fits: (1) no-production 4C fit with a confidence level (C.L.) greater than 10^{-5} , (2) a production 1C fit with a kinematic C.L. $> 10^{-3}$, and (3) χ_{BD}^2 less than five plus the minimum χ_{BD}^2 of all fits. The best fit is chosen as the one which has the minimum sum of kinematic and bubble-density χ^2 's. There are no serious ambiguities for the final state $pK^0\pi^0\pi^+$. With no cuts, 15% of all events with a best fit to $pK^0\pi^0\pi^+$ are ambiguous. With selection on a $M(K\pi\pi) < 1.5$ GeV, 9% are ambiguous. These events have a 3% ambiguity with the final-state $pK^0K^+(\bar{K}^0)$ where one of the two K^0 's is undetected, and a 5% ambiguity with $n\bar{K}^0K^+K^+$ (see Table III). In addition to 1C fit ambiguities, there is the possibility of single π^0 events being faked, for example, by poorly measured $2\pi^0$ events. To estimate this type of background, we calculate the missing mass squared for each non-(4C) event assuming $K^+p \rightarrow pK^0\pi^+$ (MM). With a further restriction to the events that the proton momentum in the lab system is less than 1 GeV/c, we obtain the missing-mass-squared distribution plotted in

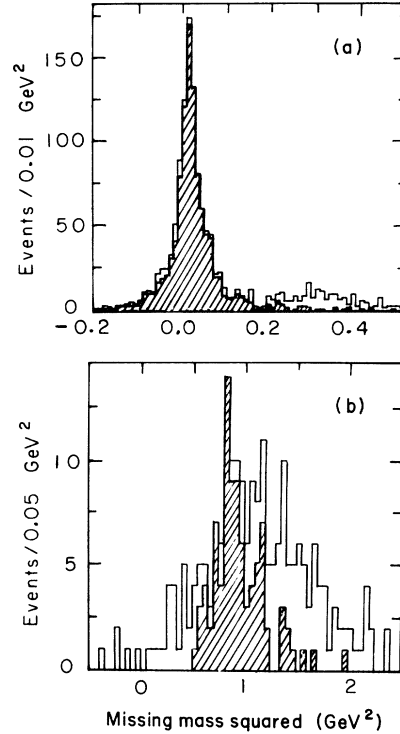


FIG. 2. The missing-mass-squared distribution for the hypotheses $K^+p \rightarrow pK^0\pi^+$ (MM) and $K^0\pi^+\pi^+$ (MM) in (a) and (b), respectively, for events with p_p^{lab} or $p_{(MM)}^{\text{lab}}$ less than 1 GeV/c. For (b) there is an additional selection on $M(K\pi\pi) < 1.5$ GeV. The shaded areas correspond, respectively, to events with best fits to $pK^0\pi^+\pi^0$ and $K^0\pi^+\pi^+n$. Figures (a) and (b) correspond to subsamples of, respectively, 25% and 90% of all vee two-prongs.

Fig. 2(a), wherein the shaded area corresponds to events which have a best fit to the final state $pK^0\pi^0\pi^+$. For a linear background under the π^0 peak, the background is less than 4% of the π^0 signal for events in the π^0 region.

The final state $nK^0\pi^+\pi^+$ has a 44% ambiguity before selection on Q events. With selection on a $M(K\pi\pi) < 1.5$ GeV, the total $nK^0\pi^+\pi^+$ ambiguity is 16%. The missing-mass-squared distribution for the hypothesis $K^+p \rightarrow K^0\pi^+\pi^+$ (MM) is plotted in Fig. 2(b) for non-(4C) events with both a MM-system momentum in the lab system less than 1 GeV/c and a $M(K^0\pi^+\pi^+)$ less than 1.5 GeV. The shaded area corresponds to events with a best fit to $nK^0\pi^+\pi^+$. We have not studied these ambiguities further since we only use the number of events to obtain an upper limit for the Q branching ratio into $K^0\pi^+\pi^+$.

III. DATA ANALYSIS

In this section we discuss (A) the $K\pi\pi$ mass spectra, (B) the $K_N(1420)$ contribution to the $K\pi\pi$ mass spectra, (C) the recoil-proton momentum

transfer, (D) the decay-plane-normal distribution, (E) the Q and $K_V(890)$ two-body angular decay distributions, and (F) the $K\pi\pi$ Dalitz plots, including our fits to them.

A. $K\pi\pi$ Mass Distributions

The major evidence we have for Q substructure is the $K\pi\pi$ mass distributions given in Figs. 1 and 3. Figure 1 corresponds to no cuts. [The shaded areas are the estimated $K_N(1420)$ contributions discussed below.] Figures 3(a) and 3(b) correspond to three cuts: $M(K\pi\pi) < 1.5$ GeV, $M(p\pi^+) > 1.5$ GeV, and in addition $-t_{pp} < 1$ GeV². In all subsequent reference to Q events or Q selection these three cuts are implicit unless otherwise specified. The shaded areas of Fig. 3 and of subsequent $K^+\pi^-\pi^+$ plots correspond to best fits which have a permutation ambiguity. The $p\pi^+$ mass cut removes events with a $\Delta^{++}(1236)$ present. By examining the baryon angular-decay distributions, we estimate that the final states $pK^+\pi^-\pi^+$ and $pK^0\pi^0\pi^+$ each have less than 2.5% of resonant $p\pi^+$ remaining.³⁸ The $K^0\pi^0\pi^+$ mass spectra have a two-peak substructure – which we label Q_L and Q_H . Any mass and width values assigned to the Q_L and

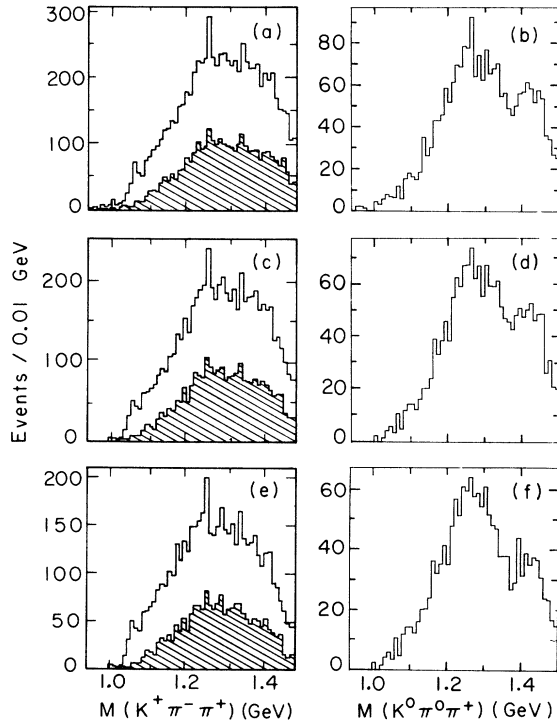


FIG. 3. The $K^+\pi^-\pi^+$ and $K^0\pi^0\pi^+$ mass spectra: (a) and (b) for $M(p\pi^+) > 1.5$ GeV and $-t_{pp} < 1$ GeV²; (c) and (d) for also $K_V(890)$ or $\rho(765)$; and (e) and (f) for $K_V(890)$ (Ref. 39). The shaded areas correspond to $K^+\pi^-\pi^+$ events with a track permutation ambiguity.

the Q_H are very background-dependent. The Q_L peaks at a mass of about 1260 MeV with a width of about 120 MeV, and the Q_H peaks at a mass of about 1420 MeV with a width of roughly 80 MeV.

The $K^+\pi^-\pi^+$ mass spectrum has a different shape from the $K^0\pi^0\pi^+$ spectrum. The effect of $K^+\pi^+$ misidentification, which washes out structure to some extent, is not large enough to explain this difference. Also, the differences in resolutions cannot account for the different shapes of the two spectra (see Table IV). However, this difference may be explained by an $\epsilon(700)K$ contribution – which is allowed for $K^+\pi^-\pi^+$, but not for $K^0\pi^0\pi^+$. By $\epsilon(700)$ we mean an $I=0$ S-wave $\pi\pi$ state and not necessarily a resonant state. One way an $\epsilon(700)K$ contribution could “fill in” the 1.36-GeV mass region is an $\epsilon(700)K$ Deck-like contribution (which peaks in this region).

We attempt to enhance substructure in the $K\pi\pi$ mass spectra by selecting on a vector meson or on t_{pp} regions. Selection on a $K_V(890)$ or $\rho(765)$ being present yields the $K\pi\pi$ mass spectra given in Figs. 3(c) and 3(d).³⁹ Figures 3(e) and 3(f) correspond to $K_V(890)$ selection. (The shaded areas correspond to events with a permutation ambiguity.) Both selections reduce the significance in the $K^0\pi^0\pi^+$ mass spectrum of the dip at 1360 MeV and reduce the 1420-MeV mass region to a flat shoulder. Thus, neither selection enhances Q substructure.

Selection on different t_{pp} regions enhances different regions of $K\pi\pi$ mass. Selecting on either $-t_{pp} < 0.1$ GeV², $0.1 < -t_{pp} < 0.3$ GeV², or $-t_{pp} > 0.3$ GeV², we obtain the $K\pi\pi$ mass distributions given in Fig. 4. Since the minimum $-t_{pp}$ is less than 0.006 GeV², our use of t_{pp} is practically equivalent to $t'_{pp} = t_{pp} - \text{mint}_{pp}$. Events in the 1260-MeV region are produced more peripherally than in the 1420-MeV region.

In addition we have examined the final-state $nK^0\pi^+\pi^+$ for a Q enhancement. The Q decay mode into $\rho(765)K$ is forbidden for this final state since

TABLE IV. FWHM (full width at half-maximum) resolutions for $K\pi\pi$ mass less than 1.5 GeV and $p\pi^+$ mass greater than 1.5 GeV.

Mass	Γ_{FWHM} (MeV)
$K^+\pi^-\pi^+$	13.0
$K^+\pi^-$	8.6
$\pi^+\pi^-$	8.0
$K^0\pi^0\pi^+$	25.6
$K^0\pi^0$	20.0
$K^0\pi^+$	9.4
$\pi^0\pi^+$	23.7

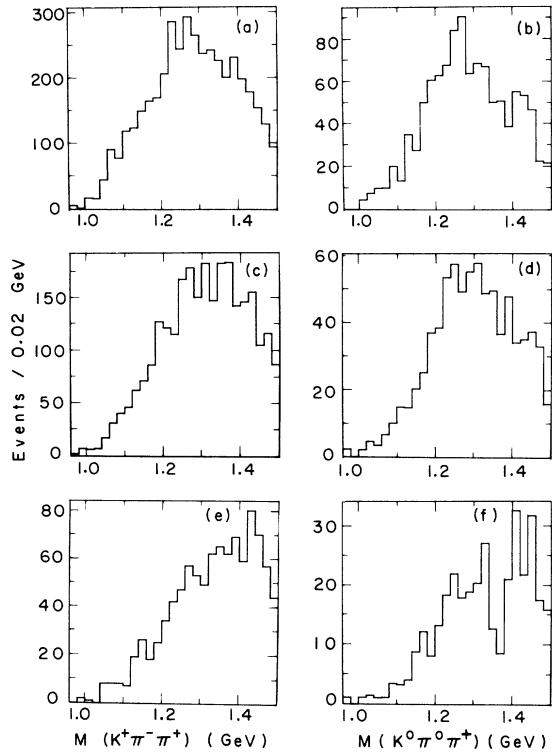


FIG. 4. The $K\pi\pi$ mass for Q events in $K^+p \rightarrow pK^+\pi^-\pi^+$ and $pK^0\pi^0\pi^+$: (a) and (b) are for $-t_{pp} < 0.1$ GeV^2 ; (c) and (d) are for $0.1 < -t_{pp} < 0.3$ GeV^2 ; (e) and (f) are for $-t_{pp} > 0.3$ GeV^2 .

$\pi^+\pi^+$ is a pure $I=2$ state. In Fig. 5 we plot the $K^0\pi^+\pi^+$ mass for events with $-t_{pn} < 1$ GeV^2 . Assuming all $K^0\pi^+\pi^+$ events in the Q region (126 events) to be pure $K_V(890)\pi$, we estimate that the $I=\frac{3}{2}K_V(890)\pi$ contribution to the Q is less than about 2% of the $I=\frac{1}{2}$ contribution wherein we have corrected for the production and decay Clebsch-Gordan isospin coefficients. We therefore agree with the accepted isospin Q assignment of $\frac{1}{2}$.

B. Contribution of the $K_N(1420)$

The $K_N(1420)$ three-body decay modes contribute to the high side of the Q mass spectra. We determine its contributions by studying the reaction $K^+p \rightarrow pK^0\pi^+$. The amounts of $K_N(1420) \rightarrow K\pi\pi$ are estimated by a two-step procedure. First, the amount of $K_N(1420) \rightarrow K^0\pi^+$ in the final-state $pK^0\pi^+$ is determined by a maximum-likelihood fit to the $K^0\pi^+$ mass spectrum. Second, the $K_N(1420)$ branching ratios are used to calculate the amounts in $K\pi\pi$.

1. Two-Body $K_N(1420)$

Before discussing the two-body fits, we note that there are no serious biases in the production

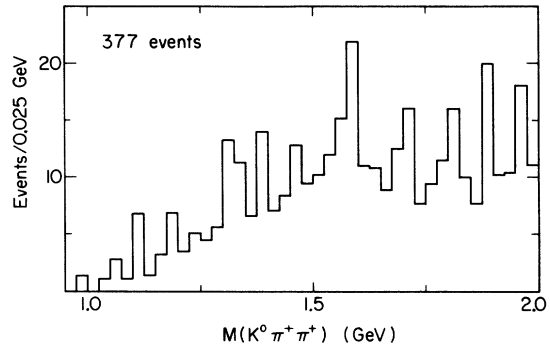


FIG. 5. The $K\pi\pi$ mass spectrum for $K^+p \rightarrow nK^0\pi^+\pi^+$ for events with $-t_{pn} < 1$ GeV^2 .

$4C$ fits to the final state $pK^0\pi^+$ for events with a $K\pi$ mass near 1420 MeV. We fit the $K^0\pi^+$ mass distribution to a D -wave Breit-Wigner and a linear background (see Fig. 6). The differential rate is given by

$$\frac{dN}{dm} = N \times B \times \left(1 + f_{\text{BW}} \frac{p_R/m_R}{p/m} \right), \quad (1)$$

where N is a total normalization constant; B is a linear background given by

$$B = 1 + s \frac{m - \bar{m}}{m_H - m_L}, \quad (2)$$

wherein $\bar{m} = \frac{1}{2}(m_L + m_H)$ and s is the slope of the background. The lower and upper mass bounds are m_L and m_H . The D -wave Breit-Wigner is given by

$$f_{\text{BW}} = \frac{r}{1-r} \frac{(\frac{1}{2}\Gamma_R) [\frac{1}{2}\Gamma(m)]}{(m-m_R)^2 + [\frac{1}{2}\Gamma(m)]^2}, \quad (3)$$

where r is the ratio of signal to signal-plus-background, m is the $K\pi$ mass, p is the K momentum in the $K\pi$ center-of-mass system, $\Gamma(m)$ is the

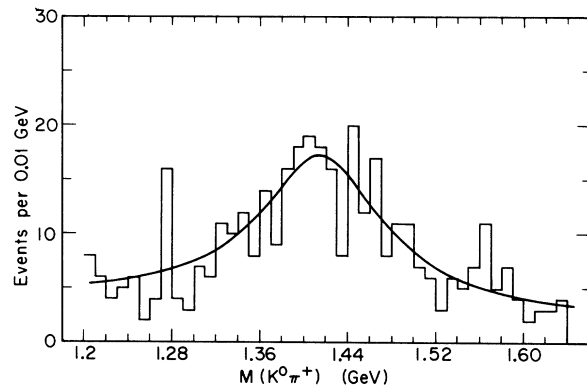


FIG. 6. The $K\pi$ mass spectrum in the 1.42-GeV region for $K^+p \rightarrow pK^0\pi^+$. The curve corresponds to a fit of the mass and width of the $K_N(1420)$, the amount of $K_N(1420)$, and a linear background as given in Table V.

TABLE V. Two-body $K_N(1420)$ fits.

A. $K^0\pi^+$ mass-plot fit over the range 1200 to 1650 MeV in 10-MeV bins			
1420 mass, m_R			1420 ± 10 MeV
1420 width, Γ_R			136^{+42}_{-30} MeV
Background slope, s			-0.65 ± 0.4
Signal to signal-plus-background ratio, r			0.81 ± 0.07
Fit χ^2			48.5
Confidence level, CL			0.14
B. Fits of $Ae^{Bt_{pp}}$ to t_{pp} plots from 0.0 to 0.4 GeV ² in 0.1-GeV ² bins			
$K\pi$ mass interval	A (events/GeV ²)	B (GeV ⁻²)	CL
(i) 1.2 to 1.35 GeV	43^{+9}_{-8}	4.0 ± 1	0.51
(ii) 1.35 to 1.50 GeV	49^{+9}_{-7}	2.3 ± 0.8	0.31
(iii) 1.50 to 1.65 GeV	22^{+7}_{-5}	2.8 ± 1.4	0.44

mass-dependent width of the resonance, and m_R , p_R , Γ_R are the corresponding resonant values. The form used for $\Gamma(m)$ is

$$\Gamma(m) = \Gamma_R \frac{[p^2/(p^2 + X^2)]^2(p/m)}{[p_R^2/(p_R^2 + X^2)]^2(p_R/m_R)}, \quad (4)$$

where X equals 100 MeV.⁴⁰ We perform a maximum-likelihood fit of m_R , Γ_R , s , and r to the $K^0\pi^+$ mass spectrum from 1200 to 1650 MeV and summarize the results in Table V. The fitted mass distribution is given in Fig. 6. The fitted number of $K_N(1420)$ is 243^{+42}_{-38} events. Our value of m_R , 1420 ± 10 MeV, agrees with the Particle Data Group's compilation value of 1408 ± 4 MeV.¹ Our value for Γ_R , 136^{+42}_{-30} MeV, agrees (within errors) with the Particle Data Group's value of 107 ± 15 MeV. If in the above fit we restrict m_R and Γ_R to the compiled values, we obtain 208 ± 30 events for the fitted amount of $K_N(1420) \rightarrow K^0\pi^+$ instead of 243^{+42}_{-38} events. Since the error for the latter amount includes the uncertainty in the values of m_R and Γ_R , we use it in the calculations for the amount of three-body $K_N(1420)$. Corrected for vee detection inefficiency the number of events is 289 ± 46 .

2. Three-Body $K_N(1420)$

The $K_N(1420)$ contributions to $K\pi\pi$ with no $p\pi^+$ mass selection can be estimated by using the above two-body amount and the $K_N(1420)$ branching ratios given by other experiments. For the $K_N(1420)$ branching ratios we use the fitted values given by the Particle Data Group: $K\pi/\text{tot} = 0.569 \pm 0.040$, $K_V(890)\pi/\text{tot} = 0.27 \pm 0.032$, and $\rho(765)K/\text{tot} = 0.092 \pm 0.035$.¹ The $K_N(1420)$ branching ratios and the observed amount of $K_N(1420) \rightarrow K^0\pi^+$ yield a prediction of 140 ± 32 events for $K_N(1420) \rightarrow K^0\pi^0\pi^+$. With additional factors for the unobserved K^0 decays and the measurement effi-

ciencies of the vee two prongs and the four prongs, the predicted amount of $K_N(1420) \rightarrow K^+\pi^-\pi^+$ is 359 ± 77 events. These predictions are indicated by the shaded areas in the uncut $K\pi\pi$ mass plots of Fig. 1. Assuming a linear background under the 1420-MeV peak, we estimate 135 ± 15 events above background in the mass range 1.36 to 1.48 GeV. In this mass range, the estimated amount of $K_N(1420)$ is 78 ± 18 so that the prediction is about 2.4 standard deviations too small.

C. t_{pp} Distributions

The t_{pp} distributions are given in Fig. 7 for Q events in $pK^+\pi^-\pi^+$ and $pK^0\pi^0\pi^+$. Since the minimum t_{pp} is less than 0.006 GeV², t_{pp} is practical-

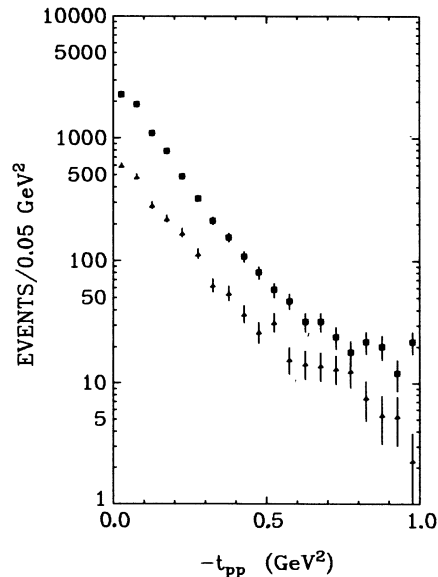


FIG. 7. The t_{pp} spectra for Q events in $K^+p \rightarrow pK^+\pi^-\pi^+$, the \blacksquare 's; and in $K^+p \rightarrow pK^0\pi^0\pi^+$, the \blacktriangle 's.

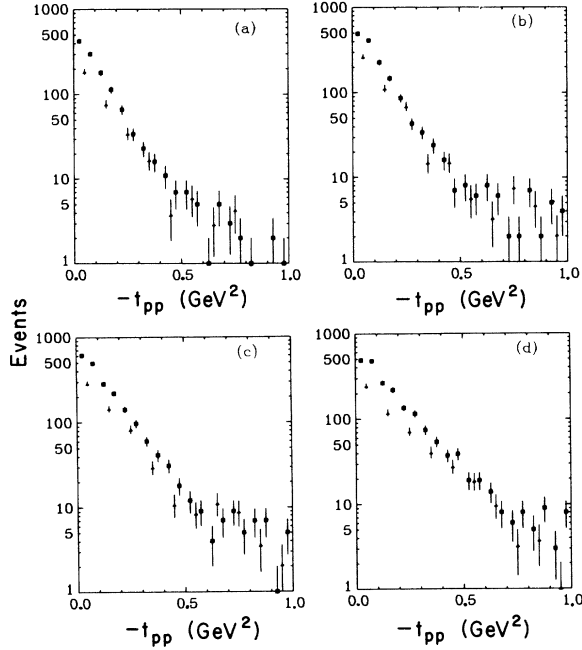


FIG. 8. The t_{pp} spectra for Q events in $K^+p \rightarrow pK^+\pi^-\pi^+$ plotted in 0.05-GeV^2 bins, the \blacksquare 's; and in $K^+p \rightarrow pK^0\pi^0\pi^+$ plotted in 0.1-GeV^2 bins, the \blacktriangle 's. (a)–(d) correspond to $K\pi\pi$ mass regions: (I) 1.1 to 1.2 GeV, (II) 1.2 to 1.27 GeV, (III) 1.27 to 1.36 GeV, and (IV) 1.36 to 1.46 GeV.

ly equivalent to $t_{pp} - \min t_{pp}$. In Fig. 8 are plotted the corresponding t_{pp} spectra for our four $K\pi\pi$ mass regions: 1.1 to 1.2 GeV, 1.2 to 1.27 GeV, 1.27 to 1.36 GeV, and 1.36 to 1.46 GeV.⁴¹ (Note in Fig. 8 that the $pK^+\pi^-\pi^+$ events are plotted with a bin size of 0.05 GeV^2 and the $pK^0\pi^0\pi^+$ events with one of 0.1 GeV^2 .) The spectra have a change of slope at $t_{pp} \cong -0.5\text{ GeV}^2$. Therefore we perform minimum χ^2 fits of $Ae^{Bt_{pp}}$ to each of these spectra over the restricted range in $|t_{pp}|$ of 0.0 to 0.4 GeV^2 . The results of these fits are summarized in Table VI. The fits to $pK^+\pi^-\pi^+$ are generally poor due to large χ^2 contributions from the first and/or second bins. As is evident from the t_{pp} distribution of $K^+\pi^-\pi^+$ for the entire Q region (see Fig. 7), a parametrization of $Ae^{Bt_{pp}}$ is inadequate and gives a very small confidence level for the fit.

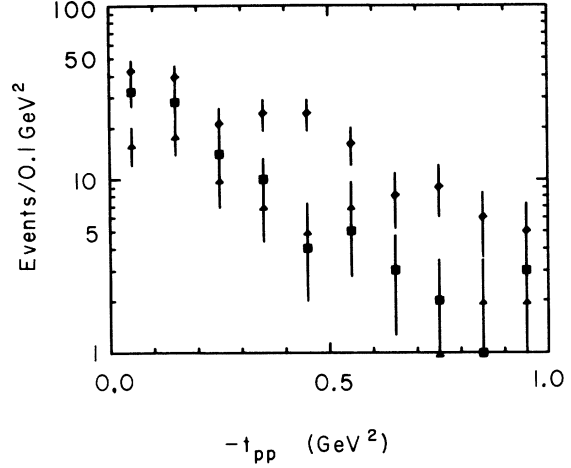


FIG. 9. The t_{pp} spectra for $K^+p \rightarrow pK^0\pi^0\pi^+$ plotted in 0.1-GeV^2 bins for $K^0\pi^+$ mass intervals: (i) 1.2 to 1.35 GeV, the \blacksquare 's; (ii) 1.35 to 1.50 GeV, the \blacklozenge 's; and (iii) 1.50 to 1.65 GeV, the \blacktriangle 's.

The $pK^0\pi^0\pi^+$ fits with poorer statistics are better, but still poor. The value of B decreases from about 9 to 6 GeV^{-2} over our four $K\pi\pi$ mass intervals. The $K^+\pi^-\pi^+$ events appear to be somewhat more peripherally produced than the $K^0\pi^0\pi^+$ events.

To estimate the contribution of the $K_N(1420)$ to the t_{pp} spectra of $K\pi\pi$ in region IV, 1.36 to 1.46 GeV, we fit $Ae^{Bt_{pp}}$ to the t_{pp} spectrum of the reaction $K^+p \rightarrow pK^0\pi^+$. To test for the possibility that the background under the $K_N(1420)$ has a different t_{pp} distribution, we perform three minimum χ^2 fits to the $K^0\pi^+$ mass intervals: (i) 1.20 to 1.35 GeV, (ii) 1.35 to 1.50 GeV, and (iii) 1.50 to 1.65 GeV. The results of these fits are summarized in Table V and the t_{pp} spectra are plotted in Fig. 9. Intervals (ii) and (iii) are in good agreement. The somewhat larger B value for interval (i) might correspond to the tail of the $K_V(890)$. Thus, we find that the background has approximately the same t_{pp} distribution as the $K_N(1420)$ which has a B value of $2.3 \pm 0.8\text{ GeV}^{-2}$.

The $K_N(1420)$ contributions to the t_{pp} spectra in

TABLE VI. Fits of $Ae^{Bt_{pp}}$ to t_{pp} spectra of $K\pi\pi$.

$M(K\pi\pi)$ region (GeV)	A in events/ GeV^2		B in GeV^{-2} (confidence level)	
	$pK^+\pi^-\pi^+$ ^a	$pK^0\pi^0\pi^+$ ^b	$pK^+\pi^-\pi^+$ ^a	$pK^0\pi^0\pi^+$ ^b
(I) 1.1 to 1.2	568 ± 27	278 ± 27	$9.5 \pm 0.4 (5.2 \times 10^{-1})$	$8.3 \pm 0.6 (8.1 \times 10^{-1})$
(II) 1.2 to 1.27	688 ± 29	394 ± 32	$9.0 \pm 0.3 (3.6 \times 10^{-3})$	$7.9 \pm 0.5 (1.6 \times 10^{-2})$
(III) 1.27 to 1.36	784 ± 29	410 ± 31	$7.6 \pm 0.3 (9.7 \times 10^{-2})$	$6.9 \pm 0.5 (2.6 \times 10^{-1})$
(IV) 1.36 to 1.46	644 ± 25	323 ± 25	$6.5 \pm 0.2 (1.2 \times 10^{-4})$	$6.1 \pm 0.5 (5.7 \times 10^{-1})$
entire Q	3014 ± 57	743 ± 27 ^a	$7.9 \pm 0.1 (1.8 \times 10^{-9})$	$6.9 \pm 0.5 (7.7 \times 10^{-2})$ ^a

^a Fits are to t_{pp} from 0.0 to 0.4 GeV^2 in 0.05-GeV^2 bins.

^b Fits are to t_{pp} from 0.0 to 0.4 GeV^2 in 0.1-GeV^2 bins.

$pK^+\pi^-\pi^+$ and $pK^0\pi^0\pi^+$ are calculated by scaling the t_{pp} spectrum of the $K\pi$ mass interval (ii) in a manner analogous to that used to estimate the $K\pi\pi$ mass contribution in Sec. IIIB 2. These estimates for $K\pi\pi$ mass region IV are plotted in Fig. 10. Though the statistics are quite poor, these estimates account for only about half of the events with $-t_{pp} > 0.5 \text{ GeV}^2$. Clearly the contribution of the $K_N(1420)$ does not change appreciably the slopes given in Table VI.

D. Q Decay-Plane Normal

If the Q were entirely diffractively produced, the Q would have unnatural spin parity and zero spin projection along the incident K . We define

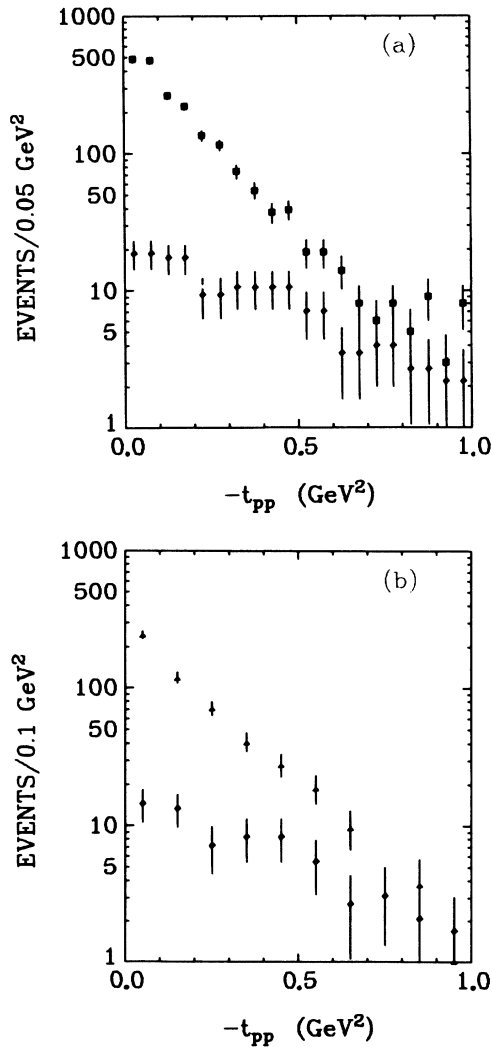


FIG. 10. In (a) and (b) the t_{pp} spectra of $K^+p \rightarrow pK^+\pi^-\pi^+$, \blacksquare , in 0.05-GeV^2 bins and $K^+p \rightarrow pK^0\pi^0\pi^+$, \blacktriangle , in 0.1-GeV^2 bins both for $1.36 < M(K\pi\pi) < 1.46 \text{ GeV}$. The \blacklozenge points are the estimated $K_N(1420)$ contributions.

axes in the Q rest frame – the beam direction as the z axis and the production-plane normal as the y axis. For $M_z = 0$ the unnatural spin parities 0^- , 1^+ , and 2^- have Q decay-plane-normal distributions of uniform, $\sin^2\Theta$, and

$$\left(\frac{g}{4} + A\right) \sin^4\Theta - 3 \sin^2\Theta + 1,$$

where Θ is the angle between the normal and the beam direction and A is a positive number.²⁵ Unnatural spin-parity states can decay into $K\pi\pi$, but not into $K\pi$; whereas natural spin-parity states can decay into both. The absence of a Q peak in the $K^0\pi^+$ mass distribution of the reaction $K^+p \rightarrow pK^0\pi^+$ (see Fig. 6) makes it plausible that the Q consists predominantly of unnatural spin-parity states except for the $K_N(1420)$ contribution of 2^+ to the high side of the Q .

For our four $K\pi\pi$ mass regions, viz., 1.1 to 1.2 GeV, 1.2 to 1.27 GeV, 1.27 to 1.36 GeV, and 1.36 to 1.46 GeV, we plot the Q decay-plane-normal $\cos\Theta$ and Φ distributions in Figs. 11 and 12. (The

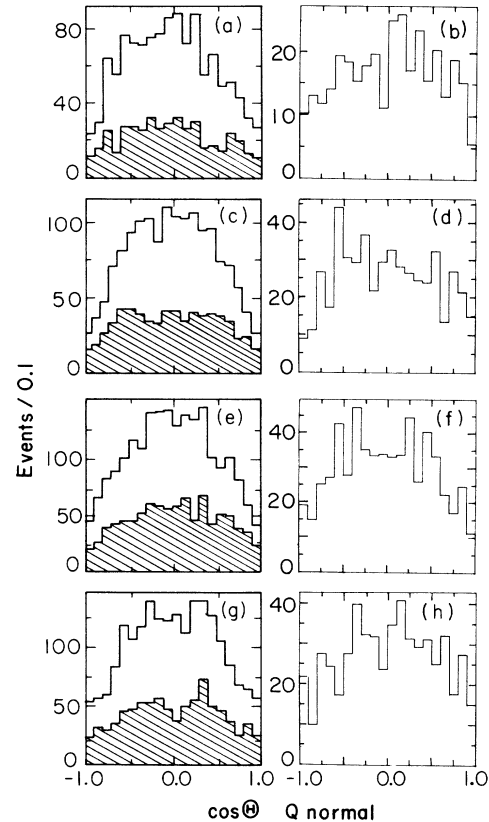


FIG. 11. The Q decay-plane-normal projection upon the beam for $K^+p \rightarrow pK^+\pi^-\pi^+$ and $pK^0\pi^0\pi^+$. (a) and (b)–(g) and (h) are for Q mass regions: (I) 1.1 to 1.2 GeV, (II) 1.2 to 1.27 GeV, (III) 1.27 to 1.36 GeV, and (IV) 1.36 to 1.46 GeV. The shaded areas correspond to $K^+\pi^-\pi^+$ events with a permutation ambiguity.

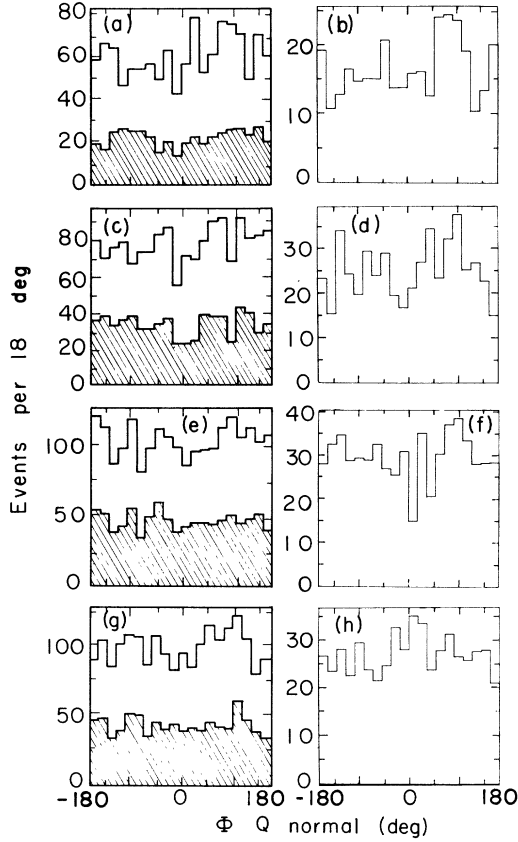


FIG. 12. The Φ distributions of the Q decay-plane normal for $K^+p \rightarrow pK^+\pi^-\pi^+$ and $pK^0\pi^0\pi^+$. (a) and (b)–(g) and (h) are for Q mass regions: (I) 1.1 to 1.2 GeV, (II) 1.2 to 1.27 GeV, (III) 1.27 to 1.36 GeV, and (IV) 1.36 to 1.46 GeV. The shaded areas correspond to $K^+\pi^-\pi^+$ events with a permutation ambiguity. The z and y axes are defined in the Q rest frame as along the beam and the production-plane normal.

shaded areas of the $K^+\pi^-\pi^+$ plots correspond to events with a permutation ambiguity.) We find the $\cos\Theta$ distributions are predominately $\sin^2\Theta$ so that the Q is predominantly 1^+ with $M_z=0$. However, the nonvanishing of the distributions near $\cos\Theta=\pm 1$ necessitates the presence of other spin states. Admixtures of 0^- , 1^+ , and 2^- with the variable A adjusted can fit the $\cos\Theta$ distributions. There is neither any striking variation in the shapes of the distributions for different $K\pi\pi$ mass regions nor any major disagreement between $K^+\pi^-\pi^+$ and $K^0\pi^0\pi^+$. All the Φ distributions are consistent with being uniform as one would expect for $M_z=0$.

The $p\pi^+$ mass cut, $M(p\pi^+) > 1.5$ GeV, suppresses events with $\cos\Theta \sim 0$; and the effects of this cut are different for $K^0\pi^0\pi^+$ and $K^+\pi^-\pi^+$ since the π^+ distribution in $K^0\pi^0\pi^+$ is different from that in $K^+\pi^-\pi^+$ due to the presence of two $K_V(890)$'s instead of one. Despite these difficulties, we bravely calculate average values of the spherical harmonics up through Y_{66} . In Table VII we list those moments which are nonzero by at least 2 standard deviations for several $K\pi\pi$ mass regions. The moment $\langle Y_{20} \rangle$ is the most significant. Furthermore, the $K^0\pi^0\pi^+$ values are systematically smaller in absolute value than the $K^+\pi^-\pi^+$ values. This effect indicates possibly different production processes for $K^0\pi^0\pi^+$ and $K^+\pi^-\pi^+$. In addition, spin states with $M_z \neq 0$ are implied by the systematically negative values of $\langle \text{Re}Y_{21} \rangle$. (A Monte Carlo calculation demonstrates that this effect is not merely due to the $p\pi^+$ mass cut.) The $L=4$ moments, which correspond in part to $J^P=2^-$ and/or 2^+ , are consistent with zero except for a slight deviation from zero of the $K^+\pi^-\pi^+$ values of $\langle \text{Re}Y_{43} \rangle$. In summary, the Q decay-plane-normal distributions

TABLE VII. Selected Q decay-plane-normal moments.

	$K\pi\pi$ mass region (GeV)			
	I (1.1 to 1.2)	II (1.2 to 1.27)	III (1.27 to 1.36)	IV (1.36 to 1.46)
$\langle Y_{20} \rangle$				
$K^+\pi^-\pi^+$	-0.087 ± 0.008	-0.099 ± 0.006	-0.087 ± 0.006	-0.082 ± 0.006
$K^0\pi^0\pi^+$	-0.059 ± 0.017	-0.062 ± 0.011	-0.073 ± 0.011	-0.056 ± 0.011
$\langle \text{Re}Y_{21} \rangle$				
$K^+\pi^-\pi^+$	-0.025 ± 0.006	-0.017 ± 0.006	-0.011 ± 0.003	-0.006 ± 0.03
$K^0\pi^0\pi^+$	-0.028 ± 0.011	-0.023 ± 0.008	-0.006 ± 0.008	-0.020 ± 0.008
$\langle Y_{40} \rangle$				
$K^+\pi^-\pi^+$	-0.005 ± 0.007	-0.002 ± 0.006	$+0.005 \pm 0.006$	0.005 ± 0.006
$K^0\pi^0\pi^+$	-0.020 ± 0.015	-0.018 ± 0.014	-0.009 ± 0.011	$+0.008 \pm 0.013$
$\langle \text{Re}Y_{43} \rangle$				
$K^+\pi^-\pi^+$	$+0.012 \pm 0.006$	-0.012 ± 0.006	-0.010 ± 0.004	-0.004 ± 0.005
$K^0\pi^0\pi^+$	0.000 ± 0.013	-0.004 ± 0.010	-0.012 ± 0.009	$+0.011 \pm 0.009$

imply the dominance of $J^P=1^+$ with $M_z=0$; but in addition there are other J^P states as well as states with $M_z \neq 0$.

E. Q and $K_V(890)$ Two-Body Angular Decays

In our analysis of the $Q \rightarrow K_V(890)\pi$ and $K_V(890) \rightarrow K\pi$ angular decay distributions we consider only the final state $pK^+\pi^-\pi^+$ for which there is just one $K_V(890)$ possible. For a Q with $J^P=1^+$, the decay into $K_V(890)\pi$ is either S wave or D wave. The S -wave decay corresponds to a uniform decay of the Q into $K_V(890)\pi$. For a Q with $J^P=1^+$ and $M_z=0$, the S -wave decay into $K_V(890)\pi$ leads to a $\cos^2\Theta_{K_V}$ decay distribution of the $K_V(890)$ into $K\pi$. We take the $K_V(890)$ and K^+ as decay indicators and define the z and y axes as along the beam and production-plane-normal in the Q rest frame. With an additional mass selection on $K_V(890)$, the $\cos\Theta_Q$ and Φ_Q distributions are given in Fig. 13 for our four $K\pi\pi$ mass regions, 1.1 to 1.2 GeV, 1.2 to 1.27 GeV, 1.27 to 1.36 GeV, and 1.36 to 1.46 GeV (Ref. 39).

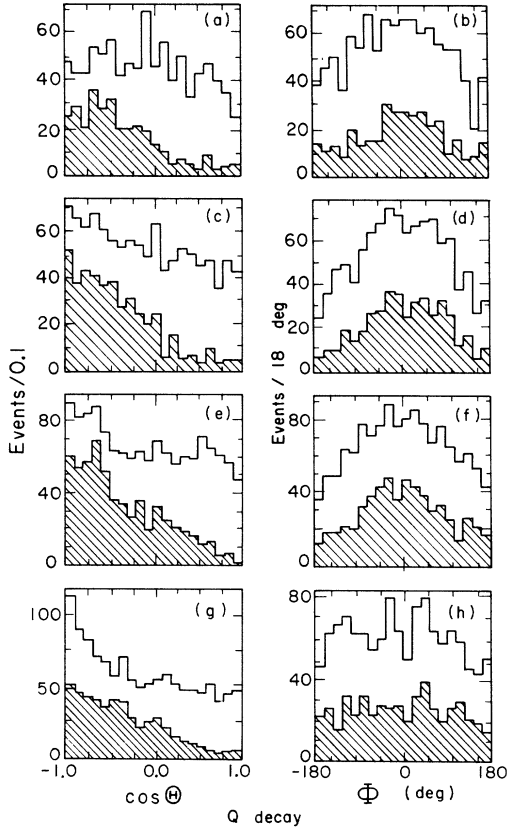


FIG. 13. The angular distributions of $Q \rightarrow K_V(890)\pi$ for $K^+p \rightarrow pK^+\pi^-\pi^+$ with $K_V(890)$ selection, where (a) and (b)–(g) and (h) are for Q mass regions: (I) 1.1 to 1.2 GeV, (II) 1.2 to 1.27 GeV, (III) 1.27 to 1.36 GeV, and (IV) 1.36 to 1.46 GeV (Ref. 39). The shaded areas correspond to events with a permutation ambiguity.

GeV, 1.27 to 1.36 GeV, and 1.36 to 1.46 GeV. The $\cos\Theta_Q$ distributions have a backward peak. Two effects complicate the interpretation of this behavior. First, the $p\pi^+$ mass cut suppresses events with $\cos\Theta_Q \sim 1$. This effect becomes broader and more pronounced for larger $K\pi\pi$ mass. Second, and more important, the observed backward peaking in $\cos\Theta_Q$ is mostly due to background, which is more pronounced for larger $K\pi\pi$ mass. The background includes $K^+\pi^+$ misidentification, $\rho(765)K$, and possibly $\epsilon(700)K$. In addition for region IV about 80 events of $K_N(1420)$ contribute to the backward peak in $\cos\Theta_Q$. These $K_N(1420)$ events have an approximately $(Y_{20})^2$ distribution in $\cos\Theta_Q$. These effects account largely for the variation in the $\cos\Theta_Q$ distributions from regions I to IV. Because of these effects and the large number of the possible contributions of the spin-parity states -0^- , S wave 1^+ with either $M_z=0$ or $M_z=\pm 1$, D wave 1^+ , 2^- , and 2^+ we do not attempt any fits.

If the Q spin states all had $M_z=0$, then the Φ_Q

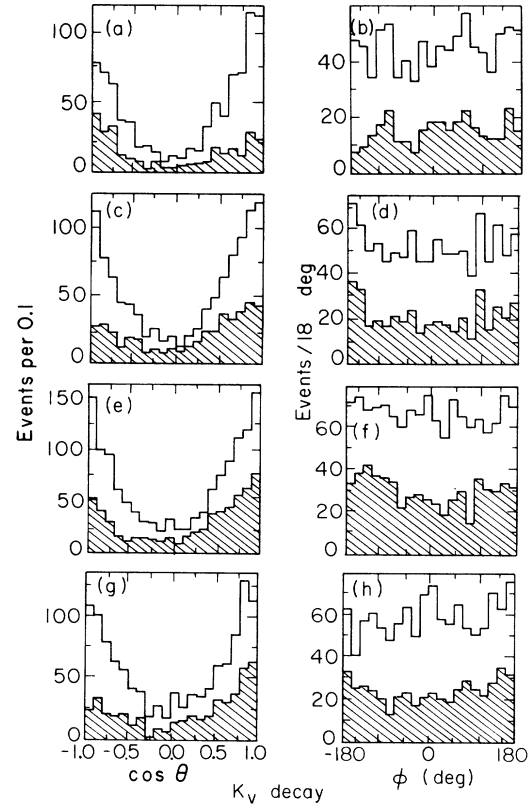


FIG. 14. The $K_V(890)$ angular-decay spectra with axes in the $K\pi\pi$ rest frame. (a) and (b)–(g) and (h) are for $K^+\pi^-\pi^+$ events in the Q mass regions: (I) 1.1 to 1.2 GeV, (II) 1.2 to 1.27 GeV, (III) 1.27 to 1.36 GeV, and (IV) 1.36 to 1.46 GeV (Ref. 39). The shaded areas correspond to events with a permutation ambiguity.

distributions would be uniform. The nonflatness of the Φ_Q distributions in Fig. 13 constitutes further support for the presence of Q spin states with $M_z \neq 0$.

The corresponding $K_V(890)$ decay distributions are given in Fig. 14. The axes are the same as before and the K^+ is taken as the decay indicator. The large positive asymmetries in the $\cos\theta_{K_V}$ distributions can be explained in terms of $K_V(890)\pi$ interfering with $\rho(765)K$. The ϕ distributions are consistent with being flat.

F. $K\pi\pi$ Dalitz Plots

In this section we present first the general features of the $K\pi\pi$ Dalitz plots and then proceed to discuss our fits.

1. General Features

The $K\pi\pi$ Dalitz plots are given in Fig. 15. For $K^+\pi^-\pi^+$ there is only one $K\pi$ combination for $K_V(890)$, while for $K^0\pi^0\pi^+$ there are two. The curves correspond to the Dalitz-plot boundary for

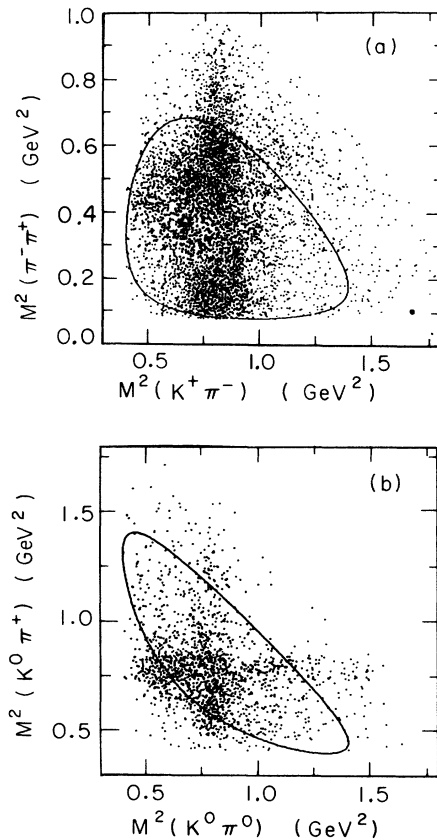


FIG. 15. The Q Dalitz plots in (a) $M^2(\pi^-\pi^+)$ vs $M^2(K^+\pi^-)$ for $K^+\pi^-\pi^+$ and in (b) $M^2(K^0\pi^+)$ vs $M^2(K^0\pi^0)$ for $K^0\pi^0\pi^+$. The curves correspond to boundaries for a $M(K\pi\pi)=1.32$ GeV.

a $K\pi\pi$ mass of 1.32 GeV. The corresponding two-body mass plots are given in Figs. 16 and 17. (The shaded areas correspond to events with a permutation ambiguity.) The $K_V(890)\pi$ contribution is dominant, but there is also a significant $\rho(765)K$ contribution.

2. Dalitz-Plot Fits

We present fits to the $K\pi\pi$ Dalitz plots for each of our four $K\pi\pi$ mass regions, 1.1 to 1.2 GeV, 1.2 to 1.27 GeV, 1.27 to 1.36 GeV, and 1.36 to 1.46 GeV. First we discuss the objectives, complications, and formalism of the fits. Secondly, we present the $K^0\pi^0\pi^+$ fits, and next the $K^+\pi^-\pi^+$ fits. Thirdly, we compare the fits and estimate

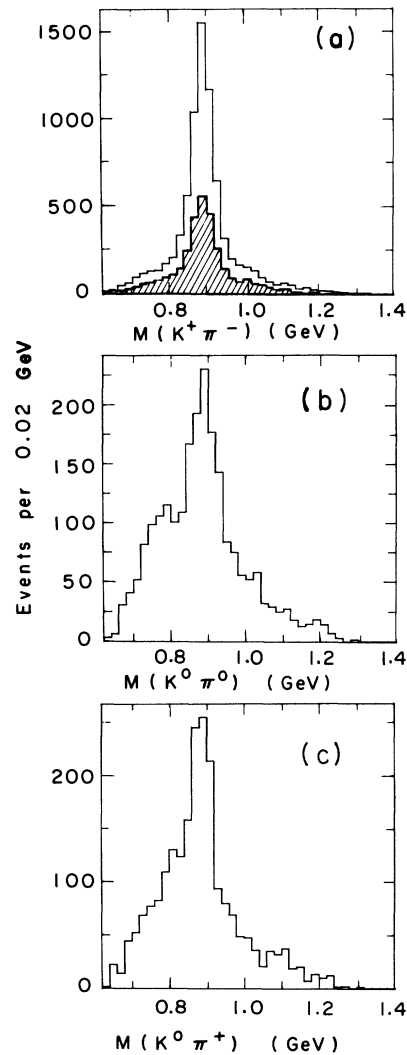


FIG. 16. $K\pi$ mass spectra when a $K_V(890)$ is possible: $K^+\pi^-$ for $K^+p \rightarrow pK^+\pi^-\pi^+$ in (a); $K^0\pi^0$ and $K^0\pi^+$ for $K^+p \rightarrow pK^0\pi^0\pi^+$ in (b) and (c). The shaded area in (a) corresponds to events with a permutation ambiguity.

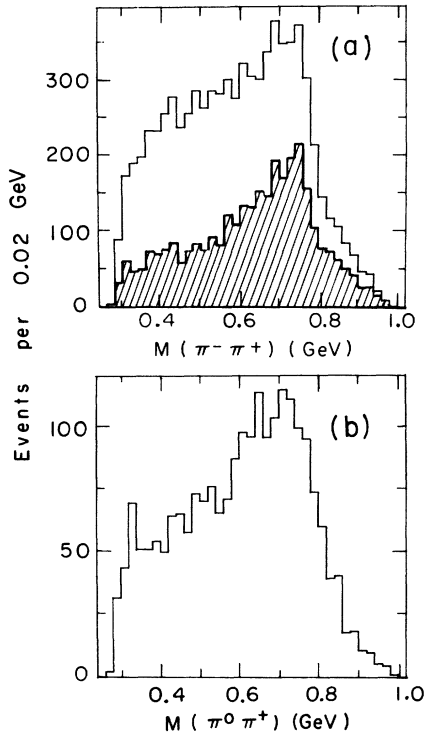


FIG. 17. The $\pi\pi$ mass spectra for Q events in (a) $K^+p \rightarrow pK^+\pi^-\pi^+$ and (b) $pK^0\pi^0\pi^+$. In (a) the shaded area corresponds to events with a permutation ambiguity.

the $\epsilon(700)K$ contribution.

a. Formalism of the fits. The objectives of the Dalitz-plot fits are to determine (1) the $\rho(765)K$ relative to $K_V(890)\pi$ contributions, (2) the consistency between the $K^0\pi^0\pi^+$ and $K^+\pi^-\pi^+$ fits, and (3) the $\epsilon(700)K$ contribution. Complications include the possible presence of D wave 1^+ in addition to the dominant S wave 1^+ as well as other spin states $-0^-, 2^-,$ and 2^+ . The $K^+\pi^-\pi^+$ fits have an additional complication due to $K^+\pi^+$ misidentification. Bearing in mind these objectives and complications, we chose to approximate the Q as S wave 1^+ $K_V(890)\pi$ and $\rho(765)K$. The $\rho(765)K/K_V(890)\pi$ branching ratios are then determined by the $K^0\pi^0\pi^+$ fits, for which there is neither $K^+\pi^+$ misidentification nor an $\epsilon(700)K$ contribution. For the $K^+\pi^-\pi^+$ fits a simple correction for $K^+\pi^+$ misidentification is calculated. The corrected $K^+\pi^-\pi^+$ fits are compared with the $K^0\pi^0\pi^+$ fits. The $\epsilon(700)K$ contribution is estimated by using the $K^0\pi^0\pi^+$ fitted results to calculate the expected amount of $K_V(890)\pi$ and $\rho(765)K$ in $K^+\pi^-\pi^+$. Any difference with the actual number of $K^+\pi^-\pi^+$ events is attributed to an $\epsilon(700)K$ contribution.

We use a formalism for an S wave 1^+ $K_V(890)\pi$ and $\rho(765)K$ decay of the Q . Expressing the Dalitz-plot intensity in terms of a density matrix, d_{ij} ,

for the $K_V(890)\pi$ and $\rho(765)K$ amplitudes, we perform two classes of fits – incoherent fits to the diagonal elements and unconstrained fits to the entire density matrix. The Dalitz-plot intensity I is fitted to²⁰

$$I = \sum_i d_{ii} |G_i|^2 + \sum_{i < j} 2[(\text{Re}d_{ij})(\text{Re}G_i^*G_j) - (\text{Im}d_{ij})(\text{Im}G_i^*G_j)] \hat{p}_i \cdot \hat{p}_j, \quad (5)$$

where the indices i and j refer to $K_V(890)\pi^+$, $\rho(765)K$, and $K_V(890)\pi^0$, respectively, for values of 1, 2, and 3. The G_i are P -wave Breit-Wigner forms for the vector-meson decays. We use the form

$$G = F \frac{[\Gamma(p_V/p)(m/m_V)]^{1/2}}{(m^2 - m_V^2) - im_V\Gamma}, \quad (6)$$

where

$$\Gamma = \Gamma_V \left(\frac{p}{p_V}\right)^3 \left(\frac{m_V}{m}\right) \quad (7)$$

with m the vector-meson mass, p the vector-meson decay-product momentum, m_V and p_V the corresponding central values, Γ_V the vector-meson width, and F the appropriate product of Clebsch-Gordan isospin coefficients for the Q and vector-meson decays. The \hat{p}_i are the vector-meson decay-product momentum directions with respect to axes fixed in the Q rest frame. The density-matrix elements d_{ij} are proportional to products of the $K_V(890)\pi$ and/or $\rho(765)K$ couplings. The d_{ij} are normalized so that the intensity, I , integrated over the Dalitz plot for a particular $K\pi\pi$ mass region equals the number of events for that particular $K\pi\pi$ mass region. For each $K\pi\pi$ mass region we define the integrated terms of Eq. (5), viz.,

$$\text{Number of events} = \sum_i X_{ii} + \sum_{i < j} (Y_{ij} + Z_{ij}), \quad (8)$$

wherein the X_{ii} are the number of events due to incoherent $K_V(890)\pi$ or $\rho(765)K$ and the Y_{ij} and Z_{ij} are the number of events associated with the real and imaginary parts of the off-diagonal interference terms.

Each Q mass band is fitted separately for $K^0\pi^0\pi^+$ and $K^+\pi^-\pi^+$. The Dalitz plots and corresponding mass plots are given in Figs. 18–20. For each mass band we perform maximum-likelihood fits. In the fits, Monte Carlo events are used to evaluate the normalization integrals.⁴² They have the same selection as do the real events, $M(p\pi^+) > 1.5$ GeV.

b. $K^0\pi^0\pi^+$ Dalitz-plot fits. For $K^0\pi^0\pi^+$ we perform two incoherent fits to the diagonal density-

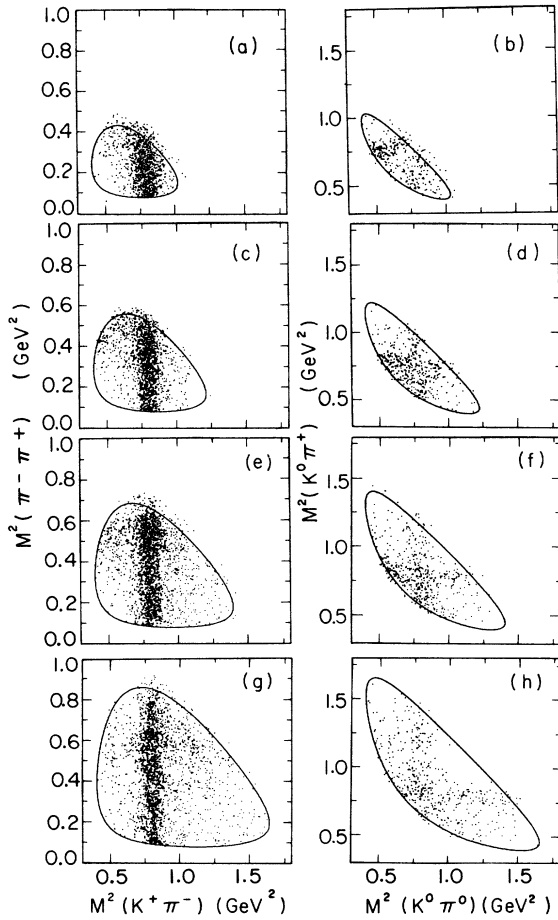


FIG. 18. Dalitz plots for $K^+\pi^-\pi^+$ and $K^0\pi^0\pi^+$ where (a) and (b)–(g) and (h) are for Q mass regions: (I) 1.1 to 1.2 GeV, (II) 1.2 to 1.27 GeV, (III) 1.27 to 1.36 GeV, and (IV) 1.36 to 1.46 GeV. The curves correspond to boundaries for $K\pi\pi$ masses of (I) 1.15 GeV, (II) 1.24 GeV, (III) 1.32 GeV, and (IV) 1.42 GeV.

matrix elements – fit No. 1 does not have the $K_V^0(890)$ and $K_V^+(890)$ couplings constrained to be equal while fit No. 2 does. Likewise we perform two fits to the entire density matrix – fit No. 3 does not have the $K_V(890)$ couplings constrained to be equal while fit No. 4 does. The unconstrained fits are a test of whether the Q corresponds to an $I=\frac{1}{2}$ state with branching ratios given by isospin Clebsch-Gordan coefficients. (The $K^0\pi^0\pi^+$ Dalitz-plot fits are to events without a t_{pp} cut. The few events with $-t_{pp} > 1$ GeV² do not appreciably change the Dalitz-plot distributions.) As is evident from the mass plots given in Figs. 19(a) and 19(b), there is for region I a greater amount of $K_V^+(890)$ than $K_V^0(890)$. The fitted d_{ij} values and the corresponding values of X , Y , and Z in Eq. (8) are given in Tables VIII and IX. The incoherent fits give fair qualitative fits, but fail in details (not shown). The fits to the entire density matrix are

quantitatively better, as evidenced by the larger values of the logarithmic likelihood, the “ $\ln w$ ” entries in the tables. Differences in the “ $\ln w$ ” values can be interpreted as one-half times the differences in the χ^2 's of the fits. The curves in Fig. 19 correspond to fit No. 4, the constrained fit to the entire density matrix. There is little difference between fits Nos. 3 and 4. In particular, the diagonal elements agree well, but the off-diagonal elements differ typically by a few standard deviations. For fit No. 3, Red_{12} and Red_{23} are in poor agreement for regions I and II.⁴³ This disagreement also indicates a larger amount of $K_V^+(890)$ than $K_V^0(890)$ for regions I and II.

There is a large $\rho(765)K$ contribution. For fit No. 2, the incoherent fit, the fraction of $\rho(765)K$ events (X_{22}/tot) has a constant value of about 0.35 ± 0.04 . Since phase space increases with increasing $K\pi\pi$ mass in the Q region more rapidly for $\rho(765)K$ than for $K_V(890)\pi$, the corresponding coupling of $\rho(765)K$ relative to $K_V(890)\pi$ decreases with increasing $K\pi\pi$ mass. For fit No. 4, the ratios of d_{22}/d_{11} are for our four $K\pi\pi$ mass regions: 1.84 ± 0.44 , 0.69 ± 0.13 , 0.43 ± 0.06 , and 0.36 ± 0.04 .

c. $K^+\pi^-\pi^+$ Dalitz-plot fits. For $K^+\pi^-\pi^+$, we perform in fit No. 5 incoherent fits to the diagonal elements of the density matrix, and in fit No. 6 we fit the entire density matrix. The incoherent fits are reasonable except for the $\pi^-\pi^+$ mass spectra (these fits are not shown). The entire density-matrix fit reproduces better the $\pi\pi$ mass spectra. (See Tables X and XI.) The curves of Fig. 20 correspond to fit No. 6. For $K\pi\pi$ regions I and II, fit No. 6 yields smaller values of d_{22} [which is proportional to the $\rho(765)K$ coupling square] than does fit No. 5, due to about an 8% constructive interference effect. All other d_{ij} of both fits agree.

Except for region I, the incoherent amount of $K_V(890)\pi$ comprises approximately 75% of the Q . However, $K^+\pi^+$ misidentification spreads out the $K^+\pi^-$ mass spectrum and peaks the $\pi^-\pi^+$ mass spectrum at about 720 MeV. As discussed before, we estimate for the entire Q about 10% of the $K^+\pi^-\pi^+$ events have the K^+ and π^+ wrongly interchanged. Since we have not determined precisely this fraction for each separate $K^+\pi^-\pi^+$ mass region or the effects of misidentification upon the fits, we assume that the fitted amount of incoherent $K_V(890)\pi$ is actually 10% low due to this bias in order to estimate an upper bound on the actual amount of $K_V(890)\pi$. From our Monte Carlo study, there is some indication that this correction is too large for region I. The errors for the corrected values do not include the uncertainty in the assumed fraction of 10%. Hence, the values quoted for $K_V(890)\pi$ could have systematic errors as

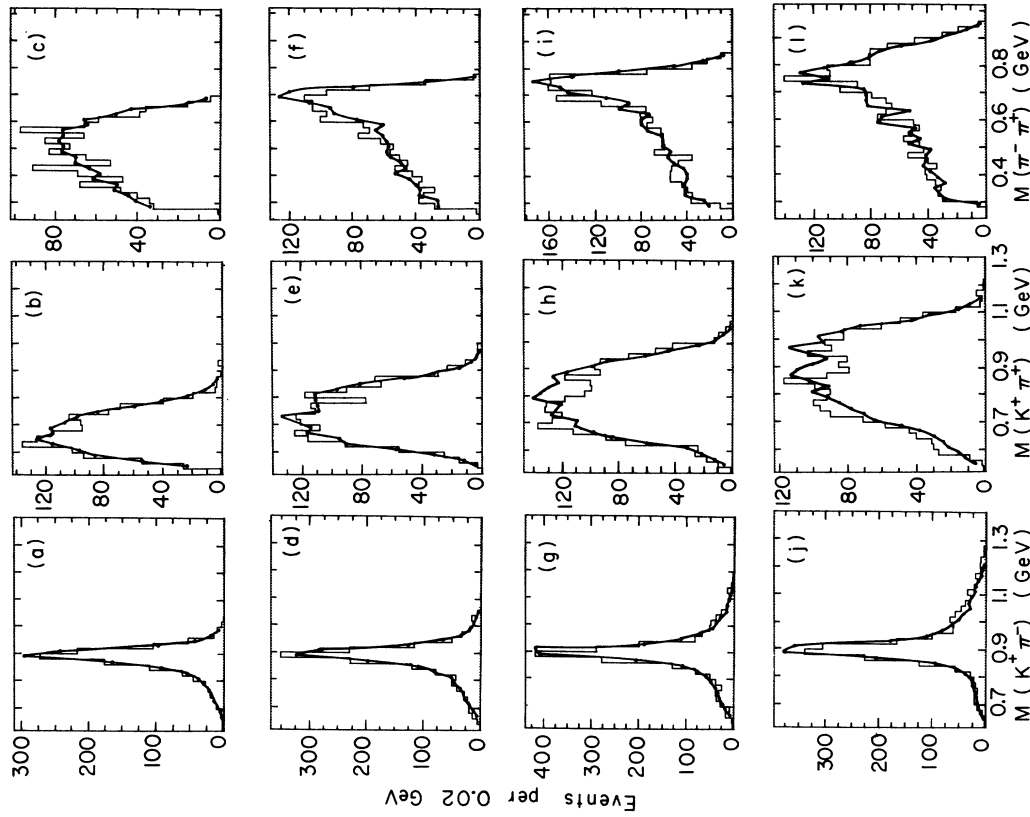


FIG. 19. The $K^0\pi^0$, $K^0\pi^+$, and $\pi^0\pi^+$ mass spectra of $K^+p \rightarrow pK^0\pi^0\pi^+$ where [(a)-(c)]-[(j)-(l)] are for Q mass regions: (I) 1.1 to 1.2 GeV, (II) 1.2 to 1.27 GeV, (III) 1.27 to 1.36 GeV, and (IV) 1.36 to 1.46 GeV. The curves correspond to the density-matrix fits described in the text (fit No. 4 of Table IX).

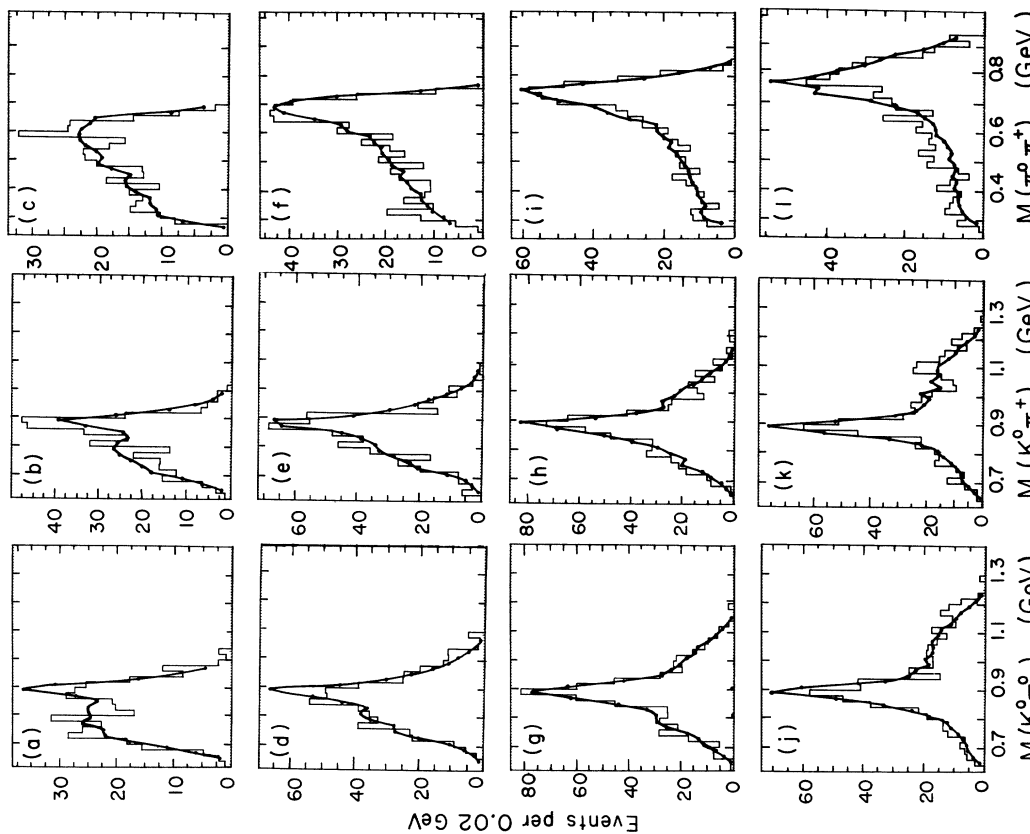


FIG. 20. The $K^+\pi^-$, $K^+\pi^+$, and $\pi^-\pi^+$ mass spectra of $K^+p \rightarrow pK^+\pi^-\pi^+$ where [(a)-(c)]-[(j)-(l)] are for Q mass regions: (I) 1.1 to 1.2 GeV, (II) 1.2 to 1.27 GeV, (III) 1.27 to 1.36 GeV, and (IV) 1.36 to 1.46 GeV. The curves correspond to the density-matrix fits described in the text (fit No. 6 of Table XI).

TABLE VIII. $K^0\pi^0\pi^+$ incoherent Dalitz-plot fits.

Fit No. 1								
$M(K\pi\pi)$ region (GeV)	Density-matrix elements ^a			Number of events ^b			Total	$\ln w$ ^c
	d_{11}	d_{22}	d_{33}	X_{11}	X_{22}	X_{33}		
(I) 1.1 to 1.2	85 ± 13	308 ± 47	113 ± 14	92 ± 14	113 ± 17	129 ± 17	334 ± 18	1668.6
(II) 1.2 to 1.27	137 ± 20	182 ± 22	171 ± 20	141 ± 21	179 ± 22	190 ± 23	509 ± 23	2799.4
(III) 1.27 to 1.36	214 ± 25	115 ± 12	188 ± 23	198 ± 23	227 ± 24	179 ± 2	604 ± 25	3508.2
(IV) 1.36 to 1.46	231 ± 25	76 ± 8	214 ± 24	183 ± 20	195 ± 21	173 ± 20	550 ± 23	3072.2

Fit No. 2								
$M(K\pi\pi)$ region (GeV)	Density-matrix elements			Number of events ^b			Total	$\ln w$
	$d_{11}=d_{33}$	d_{22}	X_{11}	X_{22}	X_{33}			
(I) 1.1 to 1.2	99 ± 9	311 ± 47	107 ± 10	114 ± 17	113 ± 11	334 ± 18	1667.4	
(II) 1.2 to 1.27	154 ± 12	182 ± 22	159 ± 12	179 ± 22	171 ± 13	509 ± 23	2798.8	
(III) 1.27 to 1.36	201 ± 15	115 ± 12	186 ± 14	227 ± 24	192 ± 14	604 ± 25	3508.0	
(IV) 1.36 to 1.46	222 ± 16	76 ± 8	176 ± 12	195 ± 21	179 ± 13	550 ± 23	3072.1	

^a The density-matrix elements d_{ij} are proportional to products of the $K_V(890)\pi$ and/or $\rho(765)K$ couplings. The indices correspond to $K_V^0(890)\pi^+$, $\rho(765)K$, and $K_V^+(890)\pi^0$ for values of 1, 2, and 3, respectively.

^b The X_{ii} are the corresponding number of events defined by Eq. (8).

^c The $\ln w$ are the logarithmic likelihoods as defined in Ref. 44.

TABLE IX. $K^0\pi^0\pi^+$ Dalitz-plot fits to the entire density matrix.

Fit No. 3 ^a										
$M(K\pi\pi)$ region (GeV)	Density-matrix elements								$\ln w$	
	d_{11}	d_{22}	d_{33}	$\text{Re}d_{12}$	$\text{Im}d_{12}$	$\text{Re}d_{13}$	$\text{Im}d_{13}$	$\text{Re}d_{23}$		$\text{Im}d_{23}$
(I) 1.1 to 1.2	95 ± 26	245 ± 55	149 ± 26	-13 ± 32	61 ± 67	122 ± 21	72 ± 32	142 ± 29	70 ± 20	1697.4
(II) 1.2 to 1.27	181 ± 31	113 ± 23	195 ± 29	22 ± 28	19 ± 39	251 ± 25	7 ± 28	90 ± 29	-4 ± 40	2856.4
(III) 1.27 to 1.36	193 ± 42	91 ± 12	231 ± 43	76 ± 25	-19 ± 24	192 ± 31	-57 ± 100	22 ± 23	-6 ± 24	3530.1
(IV) 1.36 to 1.46	262 ± 39	79 ± 10	184 ± 38	10 ± 27	37 ± 28	131 ± 47	124 ± 134	3 ± 27	18 ± 28	3079.6

$M(K\pi\pi)$ region (GeV)	Number of events									
	X_{11}	X_{22}	X_{33}	Y_{12}	Z_{12}	Y_{13}	Z_{13}	Y_{23}	Z_{23}	Total
(I) 1.1 to 1.2	103 ± 28	90 ± 20	170 ± 30	-2 ± 6	-16 ± 18	-13 ± 2	1 ± 0	23 ± 5	-21 ± 6	334 ± 18
(II) 1.2 to 1.27	187 ± 32	111 ± 22	216 ± 32	-6 ± 7	-6 ± 12	-29 ± 3	0 ± 1	23 ± 7	2 ± 1	509 ± 23
(III) 1.27 to 1.36	178 ± 39	180 ± 24	220 ± 41	23 ± 7	5 ± 6	-12 ± 2	0 ± 1	7 ± 8	2 ± 8	604 ± 25
(IV) 1.36 to 1.46	208 ± 31	203 ± 25	148 ± 30	3 ± 8	-4 ± 3	-1 ± 3	1 ± 1	1 ± 9	-3 ± 4	550 ± 23

Fit No. 4								
$M(K\pi\pi)$ region (GeV)	Density-matrix elements						$\ln w$	
	$d_{11}=d_{33}=\text{Re}d_{13}$	d_{22}	$\text{Re}d_{12}=\text{Re}d_{23}$	$\text{Im}d_{12}=\text{Im}d_{23}$	$\text{Re}d_{13}$	$\text{Im}d_{13}=0$		
(I) 1.1 to 1.2	123 ± 14	226 ± 54	67 ± 20	60 ± 43	123 ± 14	0	1684.9	
(II) 1.2 to 1.27	183 ± 16	126 ± 23	56 ± 19	16 ± 26	183 ± 16	0	2847.3	
(III) 1.27 to 1.36	213 ± 15	91 ± 12	48 ± 17	-13 ± 16	213 ± 15	0	3527.5	
(IV) 1.36 to 1.46	224 ± 16	80 ± 10	8 ± 20	22 ± 23	224 ± 16	0	3074.3	

$M(K\pi\pi)$ region (GeV)	Number of events									
	X_{11}	X_{22}	X_{33}	Y_{12}	Z_{12}	Y_{13}	Z_{13}	Y_{23}	Z_{23}	Total
(I) 1.1 to 1.2	133 ± 15	83 ± 20	141 ± 16	12 ± 4	-16 ± 12	-13 ± 1	0	11 ± 3	-18 ± 13	334 ± 18
(II) 1.2 to 1.27	189 ± 16	124 ± 23	203 ± 17	14 ± 5	-5 ± 8	-21 ± 2	0	13 ± 5	-6 ± 10	509 ± 23
(III) 1.27 to 1.36	197 ± 14	180 ± 24	203 ± 14	14 ± 5	3 ± 4	-14 ± 1	0	16 ± 6	4 ± 5	604 ± 25
(IV) 1.36 to 1.46	178 ± 13	205 ± 25	181 ± 13	2 ± 6	-3 ± 3	-13 ± 1	0	3 ± 6	-3 ± 3	550 ± 23

^a See footnotes in Table VIII.

TABLE X. $K^+\pi^-\pi^+$ incoherent Dalitz-plot fits.

$M(K\pi\pi)$ region (GeV)		Fit No. 5 ^a			Number of events		$\ln w$
		Density-matrix elements		X_{11}	X_{22}	Total	
		d_{11}	d_{22}				
(I)	1.1 to 1.2	464 ± 16	915 ± 97	999 ± 34	174 ± 18	1172 ± 34	7748.3
(II)	1.2 to 1.27	545 ± 19	785 ± 51	1099 ± 37	404 ± 26	1504 ± 39	10 318.7
(III)	1.27 to 1.36	798 ± 24	518 ± 32	1489 ± 45	533 ± 33	2023 ± 45	14 345.1
(IV)	1.36 to 1.46	937 ± 28	355 ± 24	1501 ± 45	455 ± 44	1956 ± 44	13 743.5

$M(K\pi\pi)$ region (GeV)		Fit No. 5 corrected ^b			Number of events		$\ln w$
		Density-matrix elements		X_{11}	X_{22}	Total	
		d_{11}	d_{22}				
(I)	1.1 to 1.2	516 ± 18	331 ± 100	1110 ± 38	63 ± 19	1172 ± 34	7772.4
(II)	1.2 to 1.27	606 ± 21	548 ± 52	1221 ± 41	282 ± 27	1504 ± 39	10354.9
(III)	1.27 to 1.36	887 ± 27	357 ± 33	1655 ± 51	368 ± 34	2023 ± 45	14353.5
(IV)	1.36 to 1.46	1041 ± 31	226 ± 24	1668 ± 50	288 ± 31	1956 ± 44	13745.1

^a See footnotes in Table VIII.^b We estimate a correction for $K^+\pi^+$ misidentification by increasing X_{11} by 10% and recalculating X_{22} , d_{11} , and d_{22} . The errors do not include possible systematic errors.TABLE XI. $K^+\pi^-\pi^+$ Dalitz-plot fits to the entire density matrix.

$M(K\pi\pi)$ region (GeV)		Fit No. 6 ^a				Number of events				$\ln w$	
		d_{11}	Density-matrix elements		X_{11}	X_{22}	Y_{12}	Z_{12}	Total		
			d_{22}	$\text{Re}d_{12}$	$\text{Im}d_{12}$						
(I)	1.1 to 1.2	466 ± 24	520 ± 95	442 ± 65	27 ± 133	1003 ± 52	99 ± 18	79 ± 12	-7 ± 36	1172 ± 34	7772.4
(II)	1.2 to 1.27	525 ± 23	614 ± 50	410 ± 48	91 ± 71	1059 ± 45	316 ± 26	102 ± 12	27 ± 21	1504 ± 39	10354.9
(III)	1.27 to 1.36	805 ± 26	502 ± 33	93 ± 39	100 ± 40	1503 ± 48	517 ± 34	31 ± 13	-28 ± 11	2023 ± 45	14353.5
(IV)	1.36 to 1.46	946 ± 29	346 ± 25	-40 ± 40	61 ± 40	1515 ± 46	443 ± 32	10 ± 10	7 ± 5	1956 ± 44	13745.1

$M(K\pi\pi)$ region (GeV)		Fit No. 6 corrected ^b			Number of events		$\ln w$
		Density-matrix elements		X_{11}	X_{22}	Total	
		d_{11}	d_{22}				
(I)	1.1 to 1.2	518 ± 27	-66 ± 100	1115 ± 58	-13 ± 19	1172 ± 34	7772.4
(II)	1.2 to 1.27	583 ± 25	386 ± 52	1176 ± 51	199 ± 27	1504 ± 39	10354.9
(III)	1.27 to 1.36	894 ± 29	340 ± 33	1669 ± 54	350 ± 34	2023 ± 45	14353.5
(IV)	1.36 to 1.46	1051 ± 32	215 ± 25	1684 ± 51	275 ± 32	1956 ± 44	13745.1

^a See footnotes in Table VIII.^b See footnote b in Table X.

large as 10%. We summarize the corrected values in Tables X and XI. The correction applied to the incoherent fits, fit No. 5, results in a $K_V(890)\pi$ fraction of about 0.82 ± 0.03 except for region I for which the correction gives 0.94 ± 0.03 .

Analogous to the $K^0\pi^0\pi^+$ fitted d_{22} and d_{11} values, the $K^+\pi^-\pi^+$ fitted values (both the corrected and uncorrected values) also have ratios of d_{22}/d_{11} decreasing for increasing $K\pi\pi$ mass except for the corrected values of mass region I (for which the correction is probably too large anyway).

d. Comparison of Dalitz-plot fits. In comparing the $K^0\pi^0\pi^+$ and $K^+\pi^-\pi^+$ fits, we use fits Nos. 4 and 6 since interference effects are important. In Table XII we list the d_{ij} values corrected for the

measurement efficiencies, the unseen K^0 decays, and the difference in confidence-level cutoffs for the final states $pK^0\pi^0\pi^+$ and $pK^+\pi^-\pi^+$. There are three main points. First, for $K^+\pi^-\pi^+$ and for $K^0\pi^0\pi^+$ the d_{22} values [which correspond to $\rho(765)K$ corrected for $K^+\pi^+$ misidentification] are in reasonable agreement. For region I the uncorrected d_{22} value for $K^+\pi^-\pi^+$ agrees with the d_{22} value for $K^0\pi^0\pi^+$. Secondly, the differences in $\text{Re}d_{12}$ and in $\text{Im}d_{12}$ are not significant due to the large errors, except for the $\text{Re}d_{12}$ values of regions I and II. Thirdly, there is a major disagreement in the d_{11} values. Both the corrected and uncorrected $K^+\pi^-\pi^+$ values of d_{11} which corresponds to $K_V(890)\pi$ are greater than the $K^0\pi^0\pi^+$ values, ex-

TABLE XII. Comparison of $K\pi\pi$ Dalitz-plot fits.

	$K\pi\pi$ mass region (GeV)			
	I (1.1 to 1.2)	II (1.2 to 1.27)	III (1.27 to 1.36)	IV (1.36 to 1.46)
Density-matrix element d_{11} ^a				
$K^0\pi^0\pi^+$, fit 4	453 ± 51	673 ± 57	784 ± 56	824 ± 59
$K^+\pi^-\pi^+$, fit 6	520 ± 27	585 ± 25	897 ± 29	1055 ± 32
Fit 6 corrected ^b	577 ± 30	650 ± 29	997 ± 32	1172 ± 36
Density-matrix element d_{22} ^a				
$K^0\pi^0\pi^+$, fit 4	832 ± 200	464 ± 85	335 ± 45	294 ± 36
$K^+\pi^-\pi^+$, fit 6	580 ± 105	685 ± 56	560 ± 36	386 ± 27
Fit 6 corrected ^b	-74 ± 111	430 ± 60	379 ± 37	240 ± 29
Density-matrix element $\text{Re}d_{12}$ ^a				
$K^0\pi^0\pi^+$, fit 4	247 ± 75	206 ± 69	177 ± 63	29 ± 75
$K^+\pi^-\pi^+$, fit 6	493 ± 73	457 ± 53	104 ± 44	-45 ± 44
Density-matrix element $\text{Im}d_{12}$ ^a				
$K^0\pi^0\pi^+$, fit 4	221 ± 158	59 ± 96	-48 ± 59	81 ± 83
$K^+\pi^-\pi^+$, fit 6	30 ± 148	-101 ± 79	111 ± 44	-68 ± 45

^a These entries are corrected for the measurement efficiencies and unseen K^0 's.

^b See footnote b of Table X.

cept for region II for which the values agree. Because of this disagreement it must be said that the fits disagree. Since an $\epsilon(700)K$ contribution is possible for $K^+\pi^-\pi^+$ but not for $K^0\pi^0\pi^+$, the $\epsilon(700)K$ hypothesis offers a possible simple cause for this disagreement. We do not attempt fits including $\epsilon(700)K$ because of the $K^+\pi^+$ misidentification complication.

e. $\epsilon(700)K$ contribution. Independently of any $K^+\pi^-\pi^+$ fits, the $\epsilon(700)K$ contribution in $K^+\pi^-\pi^+$ is estimated by comparing the actual number of $K^+\pi^-\pi^+$ events with the expected number of $K_V(890)\pi$ and $\rho(765)K$ events. If the Q were pure $K_V(890)\pi$, $\rho(765)K$, or $\epsilon(700)K$, then the ratio of $K^0\pi^0\pi^+$ to $K^+\pi^-\pi^+$ events would be, respectively, 1, 2, or 0. For the four mass regions, viz., 1.1 to 1.2 GeV, 1.2 to 1.27 GeV, 1.27 to 1.36 GeV, and 1.36 to 1.46 GeV, the ratios are 0.94 ± 0.07 , 1.12 ± 0.07 , 0.99 ± 0.06 , and 0.93 ± 0.06 . These ratios include corrections for the measurement efficiencies, unseen K^0 decays, and the different confidence level cutoffs. Since the $K^0\pi^0\pi^+$ fits demonstrate a significant $\rho(765)K$ contribution, the ratios imply the presence of additional $K^+\pi^-\pi^+$ events, which we attribute to $\epsilon(700)K$. By $\epsilon(700)$ we mean an $I=0$ S -wave $\pi\pi$ state and not necessarily a resonance. Of course any $\epsilon(700)K$ contribution includes both incoherent $\epsilon(700)K$ and any interference with $K_V(890)\pi$ or $\rho(765)K$. The expected number of $K^+\pi^-\pi^+$ events is determined by a Monte Carlo integration of Eq. (5) with the density-

matrix elements obtained from $K^0\pi^0\pi^+$ fit No. 4 – the fit to the entire density matrix with $K_V^+(890) = K_V^0(890)$. We attribute the difference between the actual and expected number of $K^+\pi^-\pi^+$ events as due to an $\epsilon(700)K$ contribution. We summarize our results in Table XIII. The estimated $\epsilon(700)K$ contributes to the $K^+\pi^-\pi^+$ events in our four $K\pi\pi$ mass regions the net fractions 0.15 ± 0.10 , 0.03 ± 0.08 , 0.17 ± 0.06 , and 0.22 ± 0.06 .

IV. DISCUSSION OF RESULTS

A. Summary of Results

We summarize our results and then compare them with the results obtained in three similar experiments. Our experimental results for the Q are:

(1) The $K^0\pi^0\pi^+$ mass spectrum has a two-peak substructure with one peak at about 1260 MeV with a width of about 120 MeV and a second peak at about 1420 MeV with a width of about 80 MeV. The $K^+\pi^-\pi^+$ mass spectrum has a different shape without any dip at 1360 MeV. This difference may be due to the presence of an $\epsilon(700)K$ contribution to this final state. [By $\epsilon(700)$ we mean only an $I=0$ S -wave $\pi\pi$ state.]

(2) The $K_N(1420)$ accounts for only about half of the second peak in the $K^0\pi^0\pi^+$ mass spectrum, which corresponds to a discrepancy of about 2.4 standard deviations.

(3) In agreement with the accepted Q isospin of

TABLE XIII. Comparison of total number of Q events per $K\pi\pi$ mass region.

	I (1.1 to 1.2)	II (1.2 to 1.27)	III (1.27 to 1.36)	IV (1.36 to 1.46)
$K^0\pi^0\pi^+$ observed	334 ± 18	509 ± 23	604 ± 25	550 ± 23
$K^0\pi^0\pi^+$ corrected ^a	1228 ± 77	1874 ± 101	2222 ± 113	2025 ± 106
$K^+\pi^-\pi^+$ observed	1172 ± 34	1504 ± 39	2023 ± 45	1956 ± 44
$K^+\pi^-\pi^+$ corrected ^a	1307 ± 43	1677 ± 50	2255 ± 60	2181 ± 59
Ratio of $K^0\pi^0\pi^+/K^+\pi^-\pi^+$ ^a	0.94 ± 0.07	1.12 ± 0.07	0.90 ± 0.06	0.93 ± 0.06
$K^+\pi^-\pi^+$ expected ^b	1117 ± 129	1631 ± 129	1880 ± 117	1696 ± 110
Actual minus expected	190 ± 136	46 ± 132	376 ± 132	485 ± 125

^a These entries are corrected for the measurement efficiencies and unseen K^0 's.

^b The expected number of $K^+\pi^-\pi^+$ events is calculated using the d_{ij} values obtained from $K^0\pi^0\pi^+$ fit No. 4.

$\frac{1}{2}$, the Q region of the final-state $nK^0\pi^+\pi^+$ has a cross section of $13 \pm 1 \mu\text{b}$, which corresponds to an $I = \frac{3}{2} K_V(890)\pi$ contribution to the Q of less than 2%.

(4) The Q is produced peripherally with the 1260-MeV $K\pi\pi$ mass region more peripherally produced than the 1420-MeV region.

(5) The Q decay-plane-normal spectra demonstrate that the Q is predominately in a spin-parity state of 1^+ with zero spin projection along the beam, $M_x = 0$. However, there are significant contributions of 0^- and/or 2^- and of spin states with $M_x \neq 0$. The $\langle Y_{20} \rangle$ moments of the Q decay-plane-normal are systematically smaller in absolute value for $K^0\pi^0\pi^+$ than those for $K^+\pi^-\pi^+$ in all four $K\pi\pi$ mass regions subdividing the Q . The $\langle \text{Re}Y_{21} \rangle$ moments are nonzero.

(6) The $Q \rightarrow K_V(890)\pi^+$ and the $K_V(890) \rightarrow K^+\pi^-\pi^+$ angular decay distributions imply the dominance of a 1^+ state which decays via S wave into $K_V(890)\pi$.

(7) The Q consists predominately of $K_V(890)\pi$, but also of $\rho(765)K$. For the $K^0\pi^0\pi^+$ mode, the Q is about a third $\rho(765)K$, but interference effects are important. The ratio of $K^0\pi^0\pi^+$ to $K^+\pi^-\pi^+$ events is unity to within 6% for four Q mass subdivisions. Using the $K^0\pi^0\pi^+$ fitted parameters, we estimate the amount of $K_V(890)\pi$ and $\rho(765)K$ in $K^+\pi^-\pi^+$. We find an excess of $K^+\pi^-\pi^+$ events, which we suggest is due to an $\epsilon(700)K$ contribution in $K^+\pi^-\pi^+$.

B. Comparison with Other Experiments

Our experimental results are based upon an analysis of 30 163 events of 12-GeV/c $K^+p \rightarrow pK^+\pi^-\pi^+$, reaction (1); and 6431 events of $K^+p \rightarrow pK^0\pi^0\pi^+$, reaction (2). There are three similar K^+p experiments with an incident beam momentum near 12 GeV/c. First, the Lawrence Berkeley Laboratory, Trilling-Goldhaber group (LBL-TG) have studied 7577 events of reaction (1) and 2272

events of reaction (2) at 9 GeV/c.¹⁴ Second, a collaboration of the Universities of Birmingham, Glasgow, and Oxford (BGO) has studied 7067 events of reaction (1) and 4232 events of reaction (2).²⁵ Third, a group at the University of Rochester (UR) has studied 3463 events of reaction (1) and 828 events of reaction (2) at 12.7 GeV/c.²⁷ We proceed to compare our results summarized in the previous section with each of these experiments.

1. $K\pi\pi$ Mass Spectra

LBL-TG observe a two-peak substructure for the combined events of reactions (1) and (2) – their low peak has $M_L = 1260 \pm 10$ MeV, $\Gamma_L = 40 \pm 10$ MeV and their high peak has $M_H = 1380 \pm 20$ MeV, $\Gamma_H = 120 \pm 20$ MeV [see Fig. 21(a)]. In our $K^+\pi^-\pi^+$ mass of Figs. 1 and 3, we observe a single-bin peak centered at 1265 MeV with a width of ~ 10 MeV, our resolution, but observe no dip. Our peak has a statistical significance of about 4 standard deviations. Since this peak corresponds to one bin out of 50 for the entire Q region, we do not consider it as strong evidence for narrow $K\pi\pi$ substructure.

In our $K^0\pi^0\pi^+$ mass spectrum, the peak at 1260 MeV has a width of about 120 MeV, which is significantly larger than 40 ± 10 MeV. These results are inconsistent unless there are two interfering resonances with different relative phases at the two beam momenta. Such a model has been suggested by Goldhaber.⁴⁴

BGO observe a 3σ dip at 1310 MeV in reaction (1), see Fig. 21(c). If they assume a Deck background and two incoherent resonances, they obtain in a fit to their combined data [see Fig. 21(b)] resonant masses and widths of $M_H = 1260$ MeV, $\Gamma_H = 100$ MeV, and $M_L = 1390$ MeV, $\Gamma_L = 140$ MeV. But they state that their $K\pi\pi$ mass spectra are also consistent with no substructure.

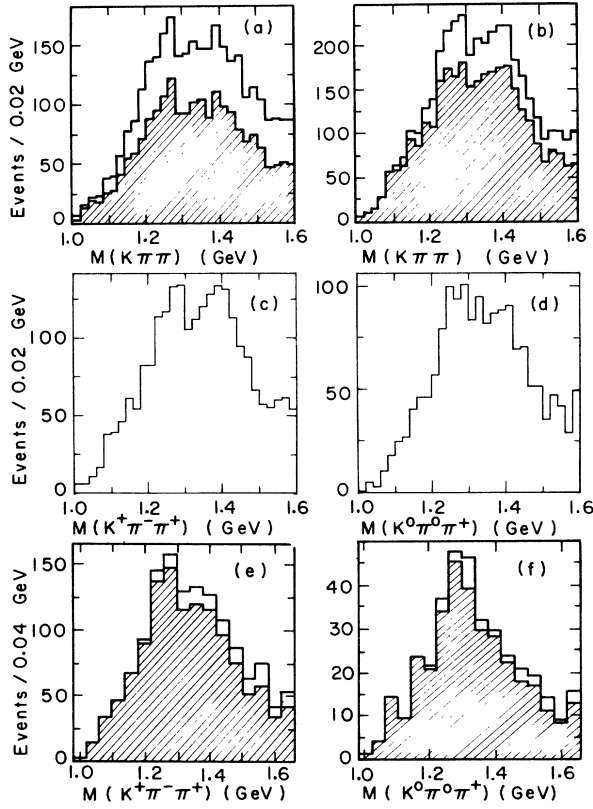


FIG. 21. The $K\pi\pi$ spectra observed by three other K^+p experiments: LBL-TG in (a), Ref. 14; BGO in (b)–(d), Ref. 25; UR in (e) and (f), Ref. 27. The shaded areas correspond to events without $\Delta^{++}(1236)$ present.

The $K\pi\pi$ mass spectra that we observe are consistent with those observed by UR [see Figs. 21(e) and 21(f)]. They parametrize their spectra as a single peak with $M = 1260 \pm 20$ MeV, $\Gamma = 180 \pm 20$ MeV, a small shoulder on the high-mass side of the Q peak, and a smooth background.

2. $K_N(1420)$ Contribution

Both LBL-TG and BGO find that the $K_N(1420)$ does not fully account for their high- Q peaks. BGO find that subtraction of $K_N(1420)$ events reduces their Q_N peak to a shoulder, but does not eliminate it [see Fig. 21(b)]. To calculate their $K_N(1420)$ contributions in $K\pi\pi$, they assume that $K_N(1420) \rightarrow K\pi\pi$ is dominated by $K_V(890)\pi$ and that the branching ratio $K\pi\pi/K\pi$ is approximately unity instead of the value 0.64 ± 0.11 which we used. They normalize the amount of $K_N(1420) \rightarrow K\pi\pi$ via the amount of $K_N(1420)$ in the reaction $K^+p \rightarrow pK^0\pi^+$. For their combined data, BGO find that the $K_N(1420)$ contributes 8 or 9% of the events in the 1.42 GeV $K\pi\pi$ mass region (1.36 to 1.46 GeV).

UR attribute the high-mass shoulder of their Q

enhancement to the $K_N(1420)$. For the reaction $K^+p \rightarrow pK_N(1420)$, $K_N(1420) \rightarrow K^0\pi^+$, they obtain a cross section of $30 \pm 7 \mu\text{b}$ with which our result of $31 \pm 5 \mu\text{b}$ agrees. When they use the $K_N(1420)$ branching ratios given in the 1969 Review of Particle Properties, which agree with the ratios used by us to within the quoted errors, they obtain an estimated $K_N(1420) \rightarrow K^+\pi^-\pi^+$ contribution of 13% in the 1420-MeV $K\pi\pi$ mass region. If instead they fix the $K_N(1420)$ mass and width at 1420 MeV and 100 MeV and vary the amount of $K_N(1420)$ along with the amount, mass, and width of a 1^+ resonance plus a fourth-order polynomial to describe the background, then they obtain about 22% for the $K_N(1420)$ contribution in the 1420-MeV $K\pi\pi$ mass region.

In comparison, we estimate that the $K_N(1420)$ contributes to $K\pi\pi$ mass region IV (1.36 to 1.46 GeV) about 15% and 9%, respectively, for reactions (1) and (2). Our estimated percentages are consistent with the value obtained by BGO. Likewise our $K^+\pi^-\pi^+$ estimate is consistent with the UR estimate based upon the $K_N(1420)$ branching ratios, but not upon their $K\pi\pi$ mass fit.

3. Isospin of Q

LBL-TG place an upper limit of 2% to an $I = \frac{3}{2}$ $K_V(890)\pi$ contribution to the Q , with which we agree. UR places an upper limit of 7 μb for $Q^{++} \rightarrow K^0\pi^+\pi^+$ in the reaction $K^+p \rightarrow nK^0\pi^+\pi^+$, $K^0 \rightarrow \pi^-\pi^+$, to be compared with our value of $(13 \pm 1) \mu\text{b}$.

4. t_{pp} Distributions

All three experiments find that the Q is peripherally produced. Fitting $e^{Bt_{pp}}$ for their combined data, BGO find that $B = 7.1 \pm 0.2 \text{ GeV}^{-2}$ for $1.2 < M(K\pi\pi) < 1.4$ GeV and that B does not depend upon $M(K\pi\pi)$ for a $M(K\pi\pi) < 1.4$ GeV, but that $B = 5.8 \pm 0.3 \text{ GeV}^{-2}$ for $1.4 < M(K\pi\pi) < 1.5$ GeV. When we fit separately reactions (1) and (2), we find similar slopes and also find a decrease in B values with increasing $K\pi\pi$ mass.

5. Q Decay-Plane-Normal Distribution

Both BGO and UR find that the Q decay-plane-normal distribution is predominantly but not entirely $\sin^2\theta$ corresponding to a Q spin parity of 1^+ with $M_z = 0$ with respect to the beam. BGO find for the Q that only the $\langle Y_{20} \rangle$ moment is consistent with being nonzero. In contrast we find that in addition to $\langle Y_{20} \rangle$ also $\langle \text{Re}Y_{21} \rangle$ is nonzero. This difference is explainable as being due to the larger statistical error in the BGO moments.⁴⁵ If the Q were purely diffractive then only spin states with $M_z = 0$ would be produced. We also observe sys-

tematically smaller absolute values of $\langle Y_{20} \rangle$ for $K^0\pi^0\pi^+$ than for $K^+\pi^-\pi^+$. This result suggests possibly different production processes for $pK^0\pi^0\pi^+$ and $pK^+\pi^-\pi^+$; possibly additional evidence for this may be seen in that our t_{pp} distributions for $Q \rightarrow K^+\pi^-\pi^+$ have somewhat steeper slopes than those for $Q \rightarrow K^0\pi^0\pi^+$.

6. Two-Body Decay of the Q

We confirm BGO's conclusion that the Q decays into $K_V(890)\pi$ by predominantly S wave. However, because of background complications we felt that we could not entirely exclude a possible D -wave contribution.

7. Q Dalitz Plot

LBL-TG fit the entire Q Dalitz plot to S wave 1^+ $K_V(890)\pi$ and $\rho(765)K$ for reactions (1) and (2) simultaneously and find that the Q decays predominantly into $K_V(890)\pi$ which interferes strongly with $\rho(765)K$. In addition they find that the ratio of $pK^0\pi^0\pi^+$ to $pK^+\pi^-\pi^+$ events in the Q equals unity. For pure $K_V(890)\pi$, $\rho(765)K$, or $\epsilon(700)K$ the ratio would be, respectively, 1, 2, and 0. Since they find a significant $\rho(765)K$ contribution, they suggest an additional $\epsilon(700)K$ contribution in $K^+\pi^-\pi^+$ as one possible explanation of this discrepancy.

In their Dalitz-plot fits to separate reactions (1) and (2), BGO include both $J^P = 1^+$ and 2^- and $\epsilon(700)K$ as well as $K_V(890)\pi$ and $\rho(765)K$ amplitudes in order to obtain agreement between their $\rho(765)K$ amplitudes of reaction (1) and reaction (2). (They also find agreement for $J^P = 1^+$ and 0^- .) Finally they state that their experimental values for $\langle Y_{20} \rangle$ and $\langle Y_{40} \rangle$ are inconsistent with the decay structure given by their Dalitz-plot fits provided that the Q is produced only with 1^+ and 2^- with $M_x = 0$ (or with 1^+ and 0^- with $M_x = 0$ only). They conclude that either the Dalitz-plot structure of a 2^- background is very different from their assumed form or that there is some production with $M_x \neq 0$.

UR obtain a good fit to their $K^+\pi^-\pi^+$ Dalitz plot with a 1^+ resonance decaying coherently into $K_V(890)\pi$ and $\rho(765)K$, a $K_N(1420)$ contribution about twice that expected upon the basis of the $K_N(1420)$ branching ratios, and, lastly, a uniform background of about $(20 \pm 10)\%$ given by phase space. They do not fit $K^0\pi^0\pi^+$ because of their low

statistics, but find the $K^+\pi^-\pi^+$ fitted parameters yield a good prediction for $K^0\pi^0\pi^+$.

Instead of attempting to include other spin parities in our Dalitz-plot fits, we have performed fits to a density matrix corresponding to only S wave 1^+ $K_V(890)\pi$ and $\rho(765)K$ amplitudes, and have obtained reasonable fits with this approximate model. We also find interference effects are important. Using our parameters determined from fits to reaction (2), we calculate the expected number of $K_V(890)\pi$ and $\rho(765)K$ events in $K^+\pi^-\pi^+$. There is an excess of $K^+\pi^-\pi^+$ events, which we suggest may be due to an $\epsilon(700)K$ contribution. However, due to the possible effects of other spin parities, which we have neglected, we consider our $\epsilon(700)K$ estimates as approximate.

Both BGO and we find that the $\rho(765)K$ coupling relative to the $K_V(890)\pi$ coupling decreases with increasing $K\pi\pi$ mass between 1.1 and 1.5 GeV. This variation is additional support for Q substructure, though it could also be due to an interference effect of a resonance with background.

C. Conclusions

In conclusion, the above results demonstrate the complexity of the Q enhancement. A meaningful resonant parametrization is difficult due to the possible contributions of the spin-parity states 0^- , D wave 1^+ , 2^- , and 2^+ in addition to the dominant S wave 1^+ . Similarly, attempts at determining the relative amounts of $K_V(890)\pi$ and $\rho(765)K$ are dependent upon the assumed J^P states and the nature of any background to the dominant $K_V(890)\pi$ and $\rho(765)K$ contributions. The observed ratio of $K^0\pi^0\pi^+$ to $K^+\pi^-\pi^+$ of unity suggests the presence of an $\epsilon(700)K$ contribution in $K^+\pi^-\pi^+$, but its precise determination is even more difficult than that of the relative amounts of $K_V(890)\pi$ and $\rho(765)K$.

ACKNOWLEDGMENTS

We gratefully acknowledge the help we received from Norman M. Uyeda and Victor Waluch. We thank Joseph J. Murray for his work in beam design and construction, the Stanford Linear Accelerator 82-in. bubble-chamber group for their assistance in data gathering, and the LBL Group A Scanning and Measuring group for their help in data reduction.

*Work done under the auspices of the U. S. Atomic Energy Commission.

¹Particle Data Group, Rev. Mod. Phys. **43**, S1 (1971).

²R. Armenteros *et al.*, Phys. Letters **9**, 207 (1964); also J. Barash *et al.*, Phys. Rev. **145**, 1095 (1966).

³D. J. Crennell, G. R. Kalbfleisch, K. W. Lai, J. M. Scarr, and T. G. Schumann, Phys. Rev. Letters **19**, 44

- (1967).
- ⁴A. Astier *et al.*, Nucl. Phys. B10, 65 (1969).
- ⁵A. Bettini *et al.*, Nuovo Cimento 62A, 1038 (1969).
- ⁶S. P. Almeida *et al.*, Phys. Letters 16, 184 (1965).
- ⁷B. C. Shen *et al.*, Phys. Rev. Letters 17, 726 (1966).
- ⁸G. Bassompierre *et al.*, Phys. Letters 26B, 30 (1967).
- ⁹J. Berlinghieri *et al.*, Phys. Rev. Letters 18, 1087 (1967).
- ¹⁰W. deBaere *et al.*, Nuovo Cimento 49A, 374 (1967).
- ¹¹J. Bartsch *et al.*, Nucl. Phys. B8, 9 (1968).
- ¹²F. Bomse *et al.*, Phys. Rev. Letters 20, 1519 (1968).
- ¹³D. Denegri *et al.*, Phys. Rev. Letters 20, 1194 (1968).
- ¹⁴G. Alexander, A. Firestone, G. Goldhaber, and D. Lissauer, Nucl. Phys. B13, 503 (1969); also G. Goldhaber, A. Firestone, and B. C. Shen, Phys. Rev. Letters 19, 972 (1967).
- ¹⁵J. Andrews *et al.*, Phys. Rev. Letters 22, 731 (1969).
- ¹⁶D. C. Colley *et al.*, Nuovo Cimento 59A, 519 (1969).
- ¹⁷J. M. Bishop *et al.*, Nucl. Phys. B9, 403 (1969).
- ¹⁸A. R. Erwin, W. D. Walker, A. T. Goshaw, and A. Weinberg, Nucl. Phys. B9, 364 (1969).
- ¹⁹J. Friedman, Lawrence Radiation Laboratory Report No. UCRL-18860, 1969 (unpublished).
- ²⁰C. Y. Chien *et al.*, Phys. Letters 29B, 433 (1969); also a Dalitz-plot analysis is given in C. Y. Chien *et al.*, *ibid.* 28B, 143 (1968).
- ²¹S. U. Chung, R. L. Eisner, N. F. Bali, and D. Lüers, Phys. Rev. 182, 1443 (1969).
- ²²B. Werner *et al.*, Phys. Rev. 188, 2023 (1969).
- ²³G. S. Abrams *et al.*, Phys. Rev. D 1, 2433 (1970).
- ²⁴P. Antich *et al.*, Nucl. Phys. B20, 201 (1970).
- ²⁵K. W. J. Barnham *et al.*, Nucl. Phys. B25, 49 (1970).
- ²⁶M. G. Bowler, Phys. Letters 31B, 318 (1970).
- ²⁷M. S. Farber, T. Ferbel, P. F. Slattery, and H. Yuta, Phys. Rev. D 1, 78 (1970).
- ²⁸A. Firestone, in *Experimental Meson Spectroscopy*, edited by C. Baltay and A. Rosenfeld (Columbia Univ. Press, New York, 1970), p. 229. Our preliminary data were included in this review.
- ²⁹A. F. Garfinkel *et al.*, Phys. Rev. Letters 26, 1505 (1971).
- ³⁰A description of the beam is given in S. Flatté, Lawrence Berkeley Laboratory Group A Physics Note No. 646, 1968 (unpublished).
- ³¹G. F. Chew and A. Pignotti, Phys. Rev. Letters 20, 1078 (1968).
- ³²S. Flatté, Lawrence Berkeley Laboratory Group A Physics Note No. 637 Rev., 1968 (unpublished).
- ³³Stephen E. Derenzo and Roger H. Hildebrand, Nucl. Instr. Methods 69, 287 (1969).
- ³⁴P. Davis and S. Flatté, Lawrence Berkeley Laboratory Group A Physics Note No. 700, 1970 (unpublished).
- ³⁵Philip J. Davis and Stanley M. Flatté, Lawrence Berkeley Laboratory Group A Physics Note. No. 724, 1971 (unpublished).
- ³⁶J. S. Danburg and G. R. Lynch, Lawrence Berkeley Laboratory Group A Programming Note. No. P-160 Rev., 1967 (unpublished).
- ³⁷For the Monte Carlo events the best fit is defined as the one with minimum χ_K^2 since the pulse heights corresponding to Spiral Reader measurements are not simulated. There is negligible difference in χ_{BD}^2 for real ambiguous events in the Q region. In our Monte Carlo generation, we use a version of PHONY modified by Norm Uyeda to use SAGE, a more efficient program for the generation of four-momenta. See the following: Philip Davis, Lawrence Berkeley Laboratory Group A Physics Note No. 184, 1969 (unpublished); E. Burns and D. Drijard, Lawrence Berkeley Laboratory Trilling-Goldhaber Group Technical Note No. 143, 1968 (unpublished); Jerome H. Friedman, J. Compt. Phys. 7, 201 (1971); see also, Jerry Friedman, Lawrence Berkeley Laboratory Group A Programming Note No. P-189 Rev., 1971 (unpublished).
- ³⁸Without selecting Q events we observe a low-mass enhancement in the $p\pi^+\pi^-$ mass spectrum near 1700 MeV as already observed in a $\pi^+p \rightarrow p\pi^+\pi^-\pi^+$ experiment at 13.1 GeV/c and reported by R. B. Willmann, J. W. Lamsa, J. A. Gaidos, and C. R. Ezell, Phys. Rev. Letters 24, 1260 (1970). However, when the Q mass region is selected this enhancement disappears. Furthermore there remains no Δ^+ enhancement in $p\pi^0$ or Δ^0 in $p\pi^-$.
- ³⁹Our $K_V(890)$ and $\rho(765)$ selections are respectively $0.84 < M(K\pi) < 0.94$ GeV and $0.65 < M(\pi\pi) < 0.85$ GeV.
- ⁴⁰Philip J. Davis, Stephen E. Derenzo, Stanley M. Flatté, Margaret A. Garnjost, Gerald R. Lynch, and Frank T. Solmitz, Phys. Rev. Letters 23, 1071 (1969).
- ⁴¹Motivated by the structure of the $K^0\pi^0\pi^+$ mass spectrum, we subdivide the Q into four $K\pi\pi$ mass regions: (I) 1.1 to 1.2 GeV, (II) 1.2 to 1.27 GeV, (III) 1.27 to 1.36 GeV, and (IV) 1.36 to 1.46 GeV.
- ⁴²We make a linear approximation to the $K\pi\pi$ mass spectrum in the integrations. A description of the program we used is given in Philippe H. Eberhard and Werner O. Koellner, Lawrence Radiation Laboratory Report No. UCRL-20159, 1970 (unpublished).
- ⁴³The indices correspond to $K_V(890)\pi^+$, $\rho(765)K$, and $K_V(890)\pi^0$ for values of 1, 2, and 3, respectively.
- ⁴⁴Gerson Goldhaber, in *Meson Spectroscopy*, edited by Charles Baltay and Arthur H. Rosenfeld (Benjamin, New York, 1968).
- ⁴⁵In the reaction $K^-p \rightarrow Q^-p$ at 10 GeV/c, the Aachen-Berlin-Bonn-CERN-Cracow-Heidelberg-London-Vienna Collaboration, Phys. Letters 34B, 160 (1971), found $\langle \text{Re}Y_{21} \rangle$ consistent with zero in the reference frame we use, with about the same statistical error as in our experiment. This was taken as evidence for t -channel helicity conservation in a $\Delta J=1$, diffractive process.